

THE UNIVERSITY OF NOTTINGHAM

**SCHOOL OF ELECTRICAL AND
ELECTRONIC ENGINEERING**



**Towards single photon detection
with a practical EMCCD**

Author: Jingsi Chen

Supervisor: Mike Somekh

**Thesis submitted to the University of Nottingham for the degree of
MSc (by research)**

DECEMBER 2009

Abstract

The stochastic transfer function (STF) is a metric for imaging of a microscope that includes the idea of noise, this project attempted to obtain the STF by Monte Carlo method with photon counting device. In this project, a very sensitive Electron-multiplying CCD (EMCCD) camera is evaluated for its photon counting performance on STF measurement. The evaluation system employs a beam with a very weak intensity laser to illuminate the EMCCD, the output signal and background noise of the EMCCD is recorded and statistical data is obtained. The EMCCD output signal distribution under different conditions is given by a simulation. Moreover, photon counting in TIRF with fluorescent beads is also carried out to simulate the practical STF measurement condition. Although the experiment results suggest that the EMCCD camera used in this project is not capable of performing photon counting for the Monte Carlo method, the performance of this EMCCD camera is studied in detail. The evaluation method and data can be used to evaluate other EMCCD or photon counting devices.

Acknowledgements

I would like to thank my supervisor Professor Mike Somekh for his invaluable help and advice throughout this year, without his support and supervision this project could not be accomplished. I would also like to thank Dr. Chung See, Dr. Mark Pitter and Gerard Byrne for their advice and support.

I would also like to thank my friends and laboratory colleagues Lin Wang, Bo Fu, Ken Hsu, Stephen, Shugang Liu and Jing Zhang for their help and support. Thanks to all other persons who provided help for the project.

Finally, I would like to thank my parents for their support and encourage throughout my study.

List of contents

Chapter 1	Introduction.....	1
1.1	Point Spread Function and Optical Transfer Function.....	3
1.1.1	Point Spread Function.....	3
1.1.2	Resolution	5
1.1.3	Optical Transfer Function	7
1.2	Stochastic transfer function and photon counting	8
1.2.1	Stochastic transfer function.....	9
1.2.2	Experimental verification for the STF.....	10
1.3	CCD.....	11
1.3.1	Structure of CCD	11
1.3.2	CCD Architecture	17
1.3.3	Noise in CCD	19
1.4	Electron-multiplying CCD (EMCCD)	22
1.4.1	Structure of EMCCD	22
1.4.2	Noise in EMCCD	23
1.5	TIRF	25
Chapter 2	Measurement system and EMCCD camera optimization.....	29
2.1	Measurement system configuration	29
2.2	Camera optimization and EM gain calibration	33
2.2.1	Camera optimization.....	34
2.2.2	EM gain calibration	39
2.2.3	Choosing a suitable EM gain value	41
Chapter 3	Evaluating photon counting performance of EMCCD	44
3.1	Principle of photon counting by EMCCD	44
3.2	Method.....	45
3.3	Result and data analysis.....	48
3.3.1	Probability density distribution	48
3.3.2	Cumulative distribution	52
3.3.3	Estimation of the CDF of one photon.....	56
3.3.4	Simulation of signal distribution	58
3.3.5	Conclusion	66
Chapter 4	Photon counting with flourophore in TIRF	68
4.1	Instrument configuration	68
4.2	Method.....	70
4.3	Analysis of results	74
Chapter 5	Conclusion	83
5.1	Summary and conclusion.....	83
5.2	Other devices which might have better performance.....	85
5.2.1	Back-illuminated EMCCD.....	85
5.2.2	PMT	87
5.2.3	ICCD.....	88
References	89

Chapter 1 Introduction

The stochastic transfer function (STF) is a metric for imaging of a microscope that includes the idea of noise. The original objective of the project was to obtain an experimental verification of STF by Monte Carlo method with an Electron-multiplying CCD (EMCCD) camera which acts as a photon counting device. The EMCCD used in the project was supposed to be very sensitive and able to perform photon counting. However, during the project the EMCCD is found to be not as sensitive as the manufacturer claims, the noise of the EMCCD became a problem in photon counting, especially at very low light intensity. Therefore the objective of the project is altered to evaluating the EMCCD for its photon counting performance on STF measurement.

A system is build to evaluate the EMCCD, in the system a beam of laser which is expanded and attenuated illuminates the EMCCD, the power of laser is measured by power meter so the photon mean number on each pixel of EMCCD during an exposure is known. The EMCCD output signal under different photon mean number and the effect of noise are studied and a simulation of probability distribution of signal and noise is performed.

Moreover, the EMCCD is used for photon counting in TIRF (Total internal reflection fluorescence microscopy) with fluorescent beads is also carried out to simulate the practical STF measurement condition. According to the

experimental results, the EMCCD camera used in this project is not capable of performing photon counting for the Monte Carlo method.

Content of the thesis:

Chapter 1: Introduction of point spread function, transfer function, stochastic transfer function, CCD, EMCCD and TIRF.

Chapter 2: The configuration of measurement system for EMCCD evaluation. The EMCCD is optimized before the experiment.

Chapter 3: The experimental method for EMCCD evaluation. The statistical data of EMCCD output signal is obtained, the probability density distribution and cumulative distribution is studied, a simulation of signal and noise probability distribution is performed based on experiment data.

Chapter 4: EMCCD photon counting in TIRF with fluorescent beads. The practical STF measurement is to be performed in TIRF with small fluorescent beads as point sources, and this experiment is to simulate photon counting in practical conditions. The experimental result obeys the previous simulation prediction.

Chapter 5: Summary and some suggestions for other photon devices.

1.1 Point Spread Function and Optical Transfer Function

1.1.1 Point Spread Function

The point spread function (PSF) describes the response of an imaging system to a point source or point object. Due to the diffraction, the image of an object formed by an optical imaging system cannot be exactly the same as the object.

A point source in an imaging system can be seen as an impulse function in linear system theory, and the PSF is an imaging system's impulse response. In a linear system, the system output is the convolution of input with system impulse response. It is similar in an imaging system, the image of a object is the convolution of the object itself with the PSF of the imaging system.

As the PSF is entirely determined by the imaging system, the degree of spreading of the PSF is a measure for the quality of an imaging system.

For a conventional light microscope, the PSF is a jinc function. The jinc function is defined as

$$\text{jinc}(x) = \frac{J_1(x)}{x} \quad (1.1)$$

where $J_1(x)$ is a Bessel function of the first kind.

The width between two first zeros of PSF is:

$$1.22 \frac{\lambda}{NA} \quad (1.2)$$

where λ is the light wavelength and NA is the numerical aperture of a microscope objective. NA is defined as the sine of the half-angle of the maximum cone of light that can enter or exit the lens multiplied by the refraction index of the medium in which the lens is working.

$$NA = n \sin q \quad (1.3)$$

It is obvious that the higher NA, the smaller width of the PSF. (Figure 1.1)

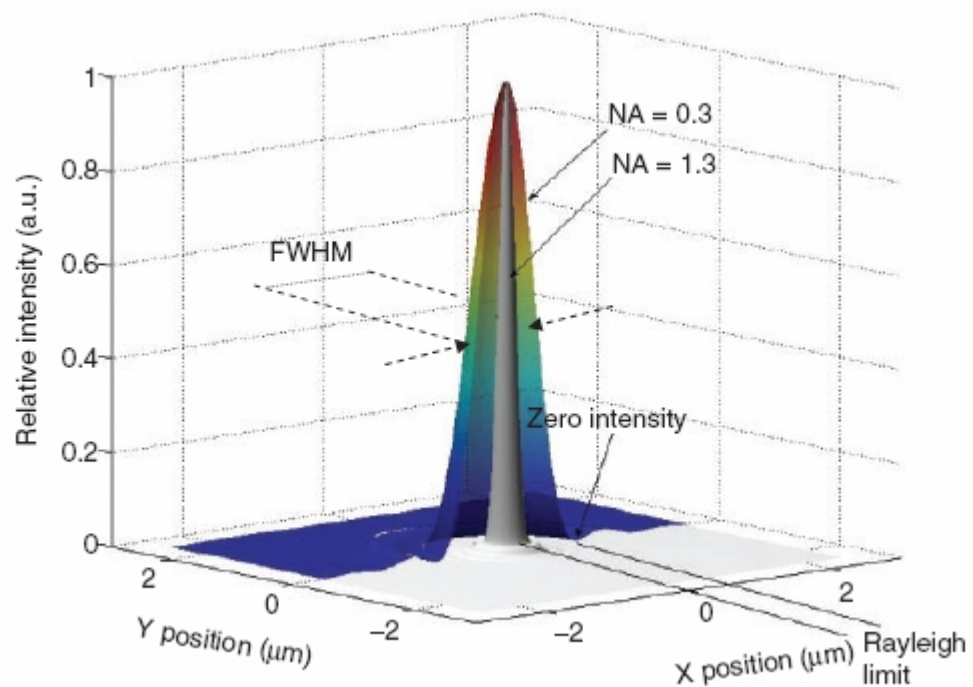


Figure 1.1 Point Spread Function (PSF), Two PSFs are shown, one for high numerical aperture (NA=1.3 in grey) and one for NA=0.3 (slightly transparent shades) [1]

1.1.2 Resolution

The resolution of a microscope objective is defined as the smallest distance between two points on a specimen that can still be distinguished as two separate entities. Resolution is a somewhat subjective value in microscopy, because the precise values of the resolution we obtained depends on the exact criterion and the signal to noise ratio (SNR).

SNR is usually not considered as a factor of resolution since the light signal is usually strong enough and SNR is usually high in normal conditions, however, when light is very weak, the SNR become an important factor of resolution. Two close points might be distinguished as two separate entities on an image with high SNR, but might not be distinguished in the case of low SNR because of the effect of noise.

The Rayleigh resolution limit defines resolution using the example of two point objects: The images of two different points are regarded as just resolved when the principal diffraction maximum of one image coincides with the first minimum of the other. If the distance is greater, the two points are well resolved and if it is smaller, they are not resolved. (Figure 1.2)

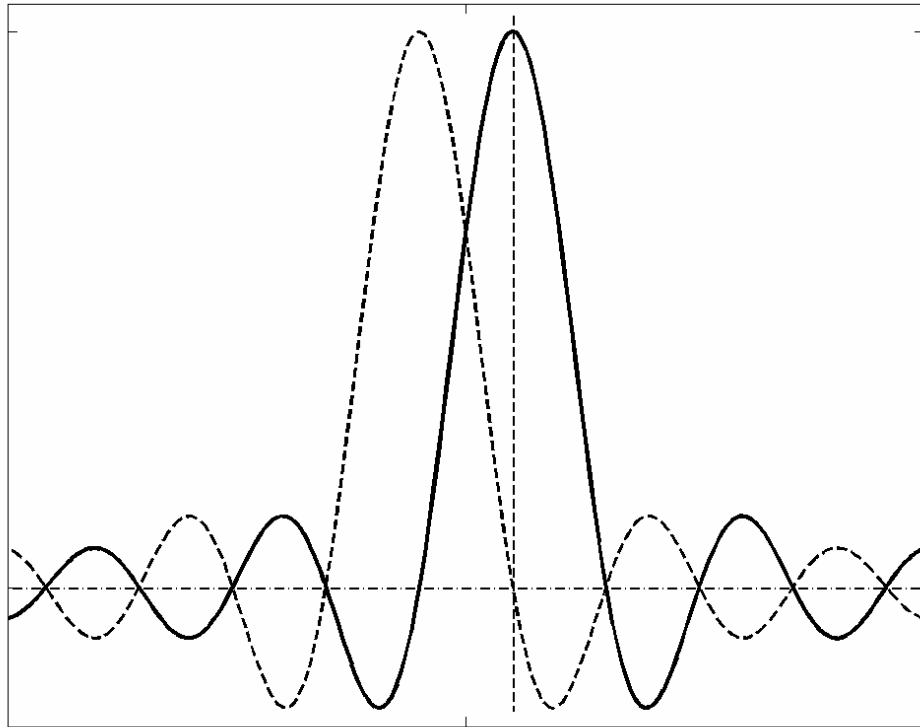


Figure 1.2 Rayleigh criterion. Two point objects are resolved when diffraction maximum of one image coincides with the first minimum of the other.

The diffraction limit given by the Rayleigh criterion is:

$$d_{\min} = 0.61 \frac{\lambda}{NA} \quad (1.4)$$

To increase the lateral resolution of the imaging system, the value of d_{\min} needs to be decreased. This can be achieved by reducing the illumination wavelength or increasing the NA of the objectives. Usually visible light is used for illumination and the wavelength ranges from about 380 to 750 nm.

As $NA = n \sin \theta$, the maximum value of $\sin \theta$ is 1, the NA of dry objective (which use air as imaging medium) cannot be greater than 1, and it is difficult to achieve NA above 0.95 in practice. For oil immersion objective, the maximum NA is usually around 1.5.

For example, at $\lambda=400\text{nm}$ using a 1.49 NA objective, the lateral resolution is about 164nm according to Rayleigh criterion.

1.1.3 Optical Transfer Function

From another point of view, an optical imaging system performs as a low pass filter in spatial frequency domain. A higher resolution means more fine detail and higher frequency component, thus a microscope system with higher resolution has a higher bandwidth.

Like a linear system, the character of an optical system can be depicted by a transfer function (or optical transfer function, OTF). The transfer function describes the spatial variation as a function of spatial (angular) frequency, it can be derived from the Fourier transform of the point spread function.

The transfer function is an important metric for microscope system. The performance a microscope can be obtained by measuring its transfer function. The transfer function can also be used to compare the performance of different microscopes

1.2 Stochastic transfer function and photon counting

As the transfer function describes the character of a microscope system, it is an important mean of comparing microscope performance. However, conventional transfer function, which is essentially the mean or average value we would expect to recover from a measurement, does not take into account the signal-to-noise ratio (SNR) which can affect image quality significantly, especially in conditions of weak signal.

For example, in the application of confocal fluorescence microscopes, a small confocal detection pinhole improves lateral resolution; however it reduces the SNR as fewer photons are detected, so this can result in a noisy image.

Since most fluorophores can only produce a finite number of photons (around 10^5 typically) before they photobleach, the trade-off between resolution and the number of photons detected is very important in fluorescence microscopy.

It is clear that an optimized microscope should not only provide good lateral resolution but also make the best possible use of the detected photons.

1.2.1 Stochastic transfer function

Recently the concept of the stochastic transfer function (STF) is introduced as a metric for imaging of a microscope that includes the idea of noise. [2]

The stochastic transfer function encapsulates the ideas by presenting a probability distribution for each spatial frequency. In contrast to the conventional transfer function which represents only the mean or expected value, the stochastic transfer function includes the noise or the variance at each spatial frequency. Ideally, it would provide a complete probability density function corresponding to each spatial frequency.

It will be very useful to have a quantitative measure of both the signal and the noise in the image, and some theoretical work [2] that leads to this idea has been done. The stochastic transfer function can be calculated in two different ways, the first method is to calculate analytically using characteristic function, and the other way is to obtain by Monte Carlo method.

In the Monte Carlo method we consider a point object, decide the total expected number of photons in the point spread function, and divide the image of PSF into small regions. For each small region, the mean value in the region is calculated, and a random number from a Poisson distribution with the expected mean value is selected. After the data of the whole PSF is collected, the data is Fourier transformed and a transfer function is obtained. The process is repeated many times so that the mean and variance

of distribution at each spatial frequency can be recovered. This process will be the exact procedure we use to extract the STF experimentally.

1.2.2 Experimental verification for the STF

The initial objective of this project was to attempt to give an experimental verification for the STF by a TIRF microscope and the procedure is very similar as described above. In the longer term it was hoped to extend it to structured light microscopy.

An image of a small fluorophore (for example, a very small fluorescent bead) formed by a microscope is divided into small segments and detected by a detector or detector array. The magnification of the image must be adjusted so that the size of the detector is small compared to the point spread function.

The detector is used in photon counting mode, and the number of photons in each small segment is recorded, and the data of photon number is Fourier transformed. The process is repeated many times, and the mean and variance of each spatial frequency is obtained from experiment result, thus the experimentally determined value of the STF could be obtained.

In this project, a very sensitive electron-multiplying CCD (EMCCD) camera, a device employs electron multiplication to amplify signal, is used for photon counting. However, in the project the performance of the

EMCCD camera appears not as good as the manufacturer claims, so the goal of the project became evaluating the performance of the EMCCD camera and determining whether it is capable of photon counting for STF measurement.

1.3 CCD

1.3.1 Structure of CCD

A CCD chip is an array of tiny light-sensitive elements called picture elements, or pixels. Pixels are defined in the silicon matrix by an orthogonal grid of narrow transparent electrode strips, or gates, deposited on the chip. A thin layer of silicon dioxide (insulator) is placed on top of the electrodes. Above the silicon dioxide is a layer of n-type silicon. Finally, a thin layer of p-type silicon lies atop the n-type silicon, this creates a p-n junction that covers the electrodes (Fig. 1.3 and 1.4). The p-n junction is reverse biased.

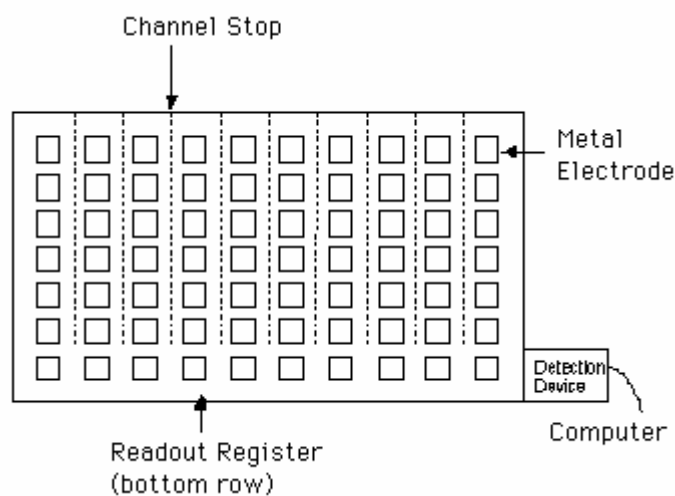


Figure 1.3 Structure of CCD

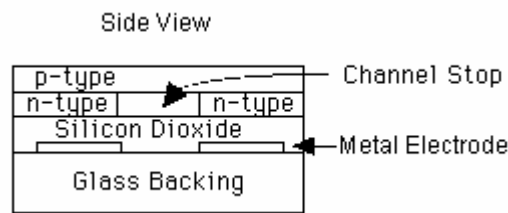


Figure 1.4 Structure of CCD, side view.

The fundamental light-sensing unit of the CCD is a metal oxide semiconductor (MOS) capacitor operated as a photodiode and storage device (Figure 1.5).

If a photon with sufficient energy is incident on the P-N junction, it can be absorbed, resulting in liberation of electrons, and an electron-hole pair is created within the silicon crystal lattice. The negatively charged electrons are collected by the positively charged gate electrode. Because one electron-hole pair is generated by one absorbed photon, the charge collected by the electrode is linearly proportional to the number of incident photons. Thus the light flux on a pixel can be determined by measuring the charge collected by the electrode.

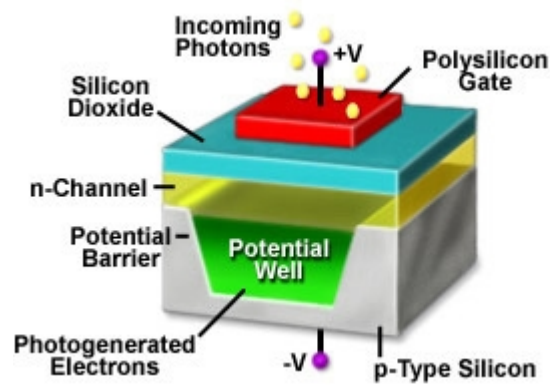


Figure 1.5 Structure of metal oxide semiconductor (MOS) capacitor. [3]

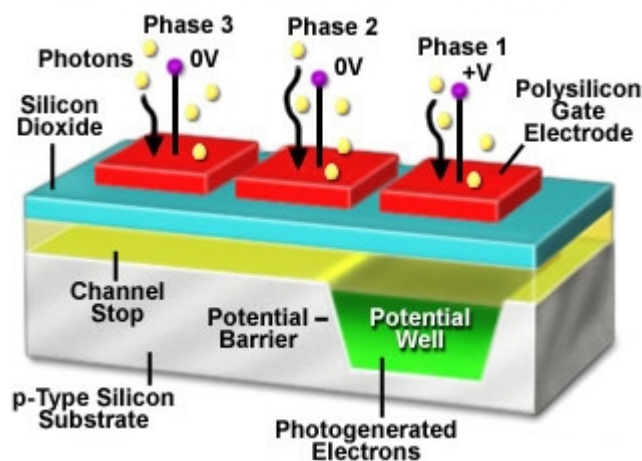


Figure 1.6 Structure of CCD sense element (pixel) [3]

After the charge created by photons is collected, it needs to be transferred and measured. During transfer, charge is moved across the device by manipulating voltages on the capacitor gates in a pattern that causes charge to spill from one MOS capacitor to the next. The shift of charge within the silicon is effectively coupled to clocked voltage patterns applied to the overlying electrode structure, the basis of the term "charge-coupled" device.

The most common charge transfer configuration is the three-phase CCD design, in which each pixel is divided into thirds with three parallel potential wells defined by gate electrodes (Figure 1.6).

Once trapped in a potential well, electrons are moved across each pixel in a three-step process (three-phase transfer) that shifts the charge packet from one pixel row to the next. A sequence of voltage changes applied to alternate electrodes of the parallel (vertical) gate structure move the potential wells and the trapped electrons under control of a parallel shift register clock, as shown in Figure 1.7.

The charge packages are vertically shifted row by row to the bottom row called the readout register, or horizontal shift register. In the horizontal shift register, charge packages are shifted one by one horizontally to output gate for amplification, measurement, and analogue-to-digital conversion (Figure 1.8).

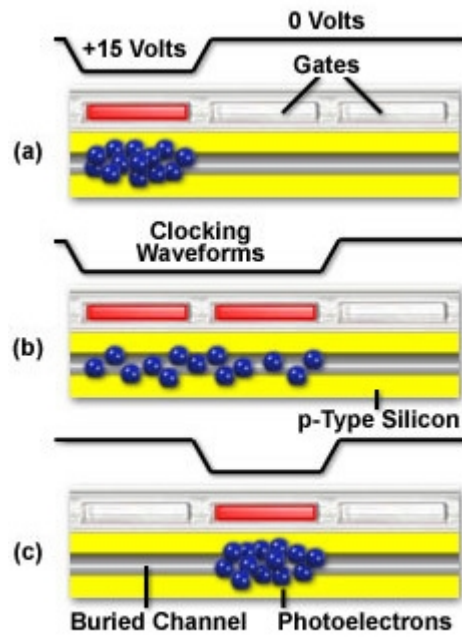


Figure 1.7 Three Phase CCD clocking schema. [3]

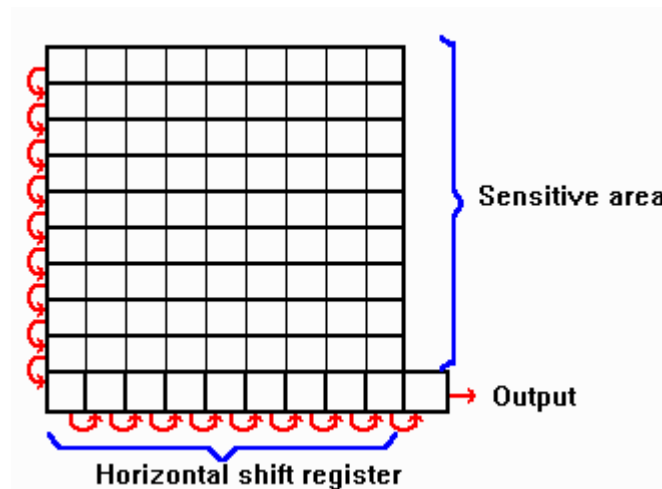


Figure 1.8 CCD readout schema. [4]

Full-well capacity

The full-well capacity of a CCD pixel is the maximum number of photoelectrons it can store before saturating. This full-well capacity determines

the maximum signal that can be sensed in the pixel, and is a primary factor affecting the CCD's dynamic range. Full well capacity is mainly determined by physical size of the individual pixel, generally, the bigger the pixel, the larger the full-well capacity.

Fill factor

Fill factor never reach to 100% as some of the sensor surface is required for control electronics. To improve the effective FF, some sensors use tiny microlenses over each pixel to gather some of the light that would otherwise have missed the photosensitive region.

Quantum efficiency

Quantum efficiency (QE) is defined as the percentage of incident photons with a particular wavelength generating electron-hole pairs which subsequently contribute to the output signal.

The parameter represents the effectiveness of a CCD imager in generating charge from incident photons, and is therefore a major determinant of the minimum detectable signal for a camera system, particularly when performing low-light-level imaging.

Conventional front-illuminated CCD normally have QE of 40-60%, with peak sensitivity normally in the range of 550-800nm, while the new back-illuminated CCD may reach maximum 90% QE.

1.3.2 CCD architecture

There are three basic variations of CCD architecture in common use: full frame, frame transfer, and interline transfer.

1.3.2.1 Full-frame CCD

The full-frame CCD, which employs the readout procedure described previously, has the advantage of high fill factor, with virtually no dead space between pixels. When full-frame CCD transfers the charge, the pixel is busy and cannot continue to capture photons. Therefore a mechanical shutter is usually used to protect the image area from incident light during readout.

The shutter is opened during exposure and charge is accumulated in pixels, then charge is transferred and read out after the shutter is closed. Because the two steps cannot occur simultaneously, image frame rates are limited by the mechanical shutter speed, the charge-transfer rate, and readout steps.

1.3.2.2 Frame-transfer CCD

Frame-transfer CCDs are similar to full-frame CCDs, but half of the array is covered by an opaque mask to provide temporary storage for the charges gathered by the unmasked light-sensitive portion. After image exposure, the charge accumulated in photosensitive pixels is quickly transferred to the storage array, typically within approximately 1 millisecond. As the storage array is covered by an opaque mask, stored charge can be read out

at a slower speed while the next image is being exposed simultaneously in light-sensitive array. Because frame-transfer CCDs are able to operate continuously without mechanical shutter, they can operate at faster frame rates than full-frame. A disadvantage of frame-transfer CCDs is that a much larger chip is required as only one-half of the surface area of the CCD is used for imaging, and larger chip also result in higher cost.

1.3.2.3 Interline CCD

In an interline CCD, each pixel has both a photo detector and a charge storage area. The storage area is formed by masking part of the pixel from light and using it only for the charge transfer process. The masked areas for each pixel form a vertical charge transfer channel that runs from the top of the array to the horizontal shift register.

Because a charge-transfer channel is located immediately adjacent to each photosensitive pixel column, charge accumulated by photosensitive pixels can be very quickly shifted to adjacent masked storage area, and then the charge can be shifted down row by row to the horizontal shift register while the image array is being exposed for the next image. Thus interline CCD can operate at high frame rate without mechanical shutter.

The disadvantage of interline CCD is that a significant portion of the sensor is no longer photosensitive, resulting in lower fill factor and hence reduced dynamic range, resolution, and sensitivity. To overcome this

problem, interline CCDs often use microlenses to increase effective fill factor.

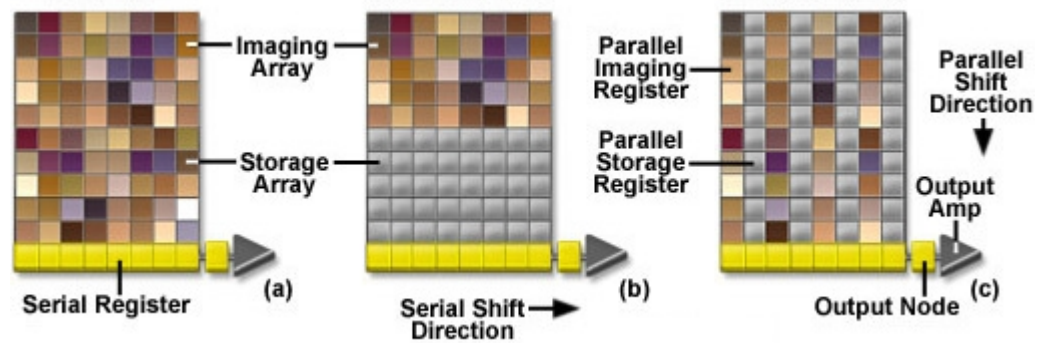


Figure 1.9 Common CCD architecture. (a) Full-frame. (b)Frame transfer. (c)Interline transfer. [3]

1.3.3 Noise in CCD

There are three main noise sources in CCDs: photon shot noise, dark current and readout noise.

1.3.3.1 Photon shot noise

Photon shot noise is an inherent noise source associated with the signal, it is due to random variations of the photon flux.

Photon shot noise obeys Poisson distribution, it is equal to the square root of the number of signal photons, N .

$$s_{SN} = \sqrt{N} \quad (1.5)$$

Since it cannot be eliminated, photon shot noise determines the maximum achievable SNR for a noise-free detector.

Signal to shot noise ratio (SSNR):

$$SSNR = \frac{N}{\sqrt{N}} = \sqrt{N} \quad (1.6)$$

It is obvious that full-well capacity is important to the SSNR. The larger full-well capacity gives a higher SSNR, provide there is sufficient light fill in the well.

1.3.3.2 Dark noise

Dark noise in CCD is noise detected in absence of light ,it is due to kinetic vibrations of silicon atoms in the CCD substrate that generate free electrons or holes even when the device is in total darkness, and it represents the uncertainty in the magnitude of dark charge accumulation during a specified time interval. The rate of generation of dark charge is termed dark current. Dark noise also follows a square-root relationship to dark current, and therefore it cannot simply be subtracted from the signal.

Dark noise is a source of noise in all semiconductor photo detectors. It can be accurately calculated for CCDs from the following equations:

$$D = 2.5 \times 10^{15} P_s N_{dc} T^{1.5} e^{-E_g/2kT} \quad (1.7)$$

where D is the dark current in electrons per sec per pixel, E_g is the silicon bandgap energy (eV), T is absolute temperature (K), P_s is the pixel size (cm^2), N_{dc} is the dark current at 300k (nA/ cm^2 , supplied by the manufacturer) and k is Boltzmann's constant (8.62×10^{-5} eV/K).

Dark current is unrelated to photon-induced signal but is highly temperature dependent, so cooling the CCD has a dramatic effect on reducing dark current. At -30 degrees, dark noise is reduced to 0.1~1 electron per pixel per second, and it is negligible for microscopy applications.

1.3.3.3 Readout noise

When the signal on CCD is read out, charge packages are converted to voltage signal and amplified. The noise in any amplifier is proportional to $B^{1/2}$, where B is system bandwidth. Generally, readout noise increases with the speed of read out. Although the readout noise is added uniformly to every pixel of the detector, its magnitude cannot be precisely determined, but only approximated by an average value, in units of electrons (root-mean-square or rms) per pixel.

Some good quality CCDs have readout noise less than 20 electrons. In this case, photon shot noise, rather than readout noise, is a dominant noise source when the signal is not very weak.

For extremely weak signals, this readout noise becomes a main noise source, and some technology, such as ICCD and EMCCD can be used to overcome the problem of readout noise in weak signal detection.

1.4 Electron-multiplying CCD (EMCCD)

1.4.1 Structure of EMCCD

EMCCD is a CCD with a multiplication register which is placed between the shift register and the output amplifier. Most EMCCDs utilize a frame transfer CCD structure shown in figure 1.10. The multiplication register contains several hundreds of elements, and it is clocked at a higher than usual voltage. This causes 'impact ionization' as the charge is transferred (Figure 1.11). Impact ionization occurs when a charge has sufficient energy to create another electron-hole pair and hence a free electron charge in the conduction band can create another charge. Hence amplification occurs, and each element of multiplication register acts as an amplifier.

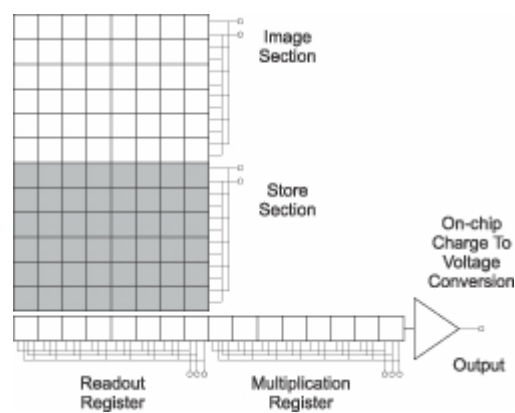


Figure 1.10 EMCCD structure schema. [5]

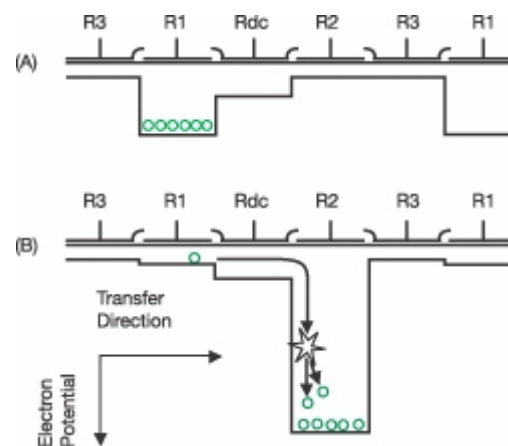


Figure 1.11 ‘Impact ionization’ in EMCCD multiplication register. [5]

The gain at each element of the multiplication register is very small (gain probability $P < 2\%$), but as the number of elements is large ($N > 500$), the cumulative effect of many elements allows very high gain ($g = (1 + P)^N$).

As each image electron is amplified to several hundred or thousand before it is read out by the output amplifier, readout noise is effectively eliminated.

1.4.2 Noise in EMCCD

Most EMCCDs are deeply cooled when operating so the dark current can be neglected, and the readout noise is overcome by electron multiplication. However, the EMCCD has some types of noise which normal CCD does not have.

1.4.2.1 Noise Factor

For a given gain setting there are fluctuations in the actual gain obtained, because the gain that is applied in the gain register is stochastic. However, the probability distribution of output charges for a given input charge can be calculated.

Figure 1.12 is a plot of the probability of output charge for various input charges for a typical EM gain set to 500. As shown in the figure, if an output signal of 1,000 electrons is obtained, there is a reasonable probability that this signal could have resulted from either an input signal of 1, 2, 3, 4 or even 5 electrons.

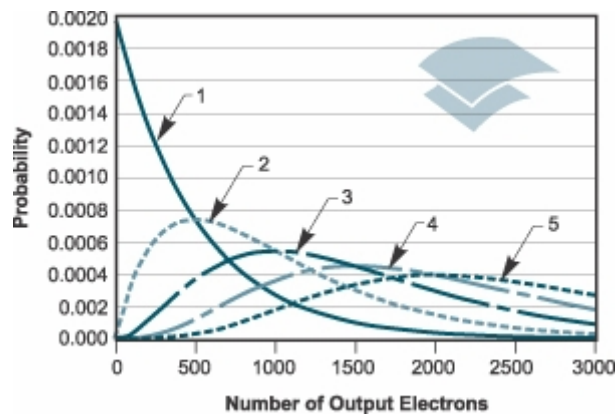


Figure 1.12 Probability of EMCCD output charge. [5]

However, at very low light levels when there is less than 1 electron falling on a pixel in a single exposure on average, it can be assumed that a pixel either contains an electron or not. In this case EMCCD can be used in

photon counting mode, in this mode a threshold is set above the ordinary amplifier readout and all events are counted as single photons. This removes the noise associated with the stochastic multiplication at the cost of counting multiple electrons in the same pixel as a single electron.

1.4.2.2 Spurious noise (or Clock Induced Charge)

The Spurious Noise or Clock Induced Charge (CIC) is created when charge is shifted pixel to pixel towards the output amplifier in CCD. There is a very small but finite probability that charges can knock off additional charges by impact ionization during charge shift. These unwanted charges become an additional noise component.

In a normal CCD the noise component is so low and it typically is hidden by the readout noise or dark current. In an EMCCD however, spurious charges that occur in the image section are amplified by the EMCCD gain register and therefore are very detectable. Thus it is essential to minimize spurious charges in very low light imaging applications such as photon counting.

1.5 TIRF

Total internal reflection fluorescence microscopy (TIRF) excite fluorescent probes very near the substrate (within $\leq 100\text{nm}$). When light travel from a higher refractive index medium (for example, glass) to a lower refractive

index medium (for example, water), the light is totally reflected by the interface if incident angle is greater than the critical angle. An exponentially decaying electromagnetic field called an 'Evanescent Wave' is created in the lower refractive index medium and propagates parallel to the interface. The intensity of the evanescent wave exponentially decays with perpendicular distance from the interface, it typically penetrates between 50nm and 200nm into the lower refractive index medium, the depth depends on media refractive indices, incident angle, and wavelength.

Because the evanescent wave selectively illuminates a very thin layer of region direct above the substrate, TIRF can provide very high contrast images of cell membrane with very low background fluorescence compared with conventional fluorescence microscopy. The TIRF technique has been used widely in different application, including studies of the topography of cell–substrate contacts [6,7,8]; measuring dynamics [9] or self-association [10] of proteins at membranes; and imaging of endocytosis or exocytosis [11,12].

There are two main types of optical configuration for TIR, prism based and prismless configuration [13]. In prismless configuration, a high numerical aperture microscope objective is used for both TIR illumination and emission observation. While prism based configuration use a prism to direct the light toward the TIR interface with a separate objective for emission observation. (Figure 1.13)

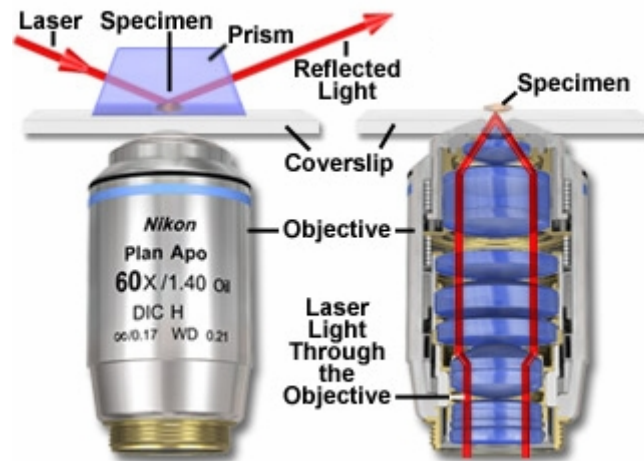


Figure 1.13 Prism based and prismless configuration of TIRF. [14]

In prismless TIRF configuration, evanescent wave illumination is achieved by focusing a laser beam to a point at the back focal plane (BFP) of the objective lens. Thus the light emerges from the objective in a collimated form, which ensures that all the rays are incident on the sample at the same angle with respect to the optical axis. The point of focus in the back focal plane is adjusted to be off-axis. At a sufficiently high off-axis radial distance, the critical angle for TIR can be exceeded and evanescent wave is created on the interface. The beam can emerge into the immersion oil (refractive index n_{oil} , shown in figure 1.14) at a maximum possible angle θ_m measured from the optical axis) given by:

$$NA = n_{oil} \sin\theta_m \quad (1.8)$$

According to Snell's Law, $n \sin\theta$ is conserved when the beam traverses through planar interfaces from one medium to the next, so we have:

$$n_{oil} \sin\theta_m = n_2 \sin\theta_2 \quad (1.9)$$

(Where subscript 2 refers to coverslip substrate on which the cells grow). In practical condition the refractive index n_{oil} and n_2 are usually very close. For total internal reflection to occur at the interface with an aqueous medium of refractive index n_1 , θ_2 must be greater than the critical angle θ_c as calculated from:

$$n_1 = n_2 \sin\theta_c \quad (1.10)$$

From the three equations above, it is obvious that the NA of objective lens must be greater than n_1 (refractive index of aqueous medium) for prismless TIR configuration. Since $n_1=1.33$ for water, and 1.37 for typical cell cytoplasm, a high numerical aperture ($NA>1.4$) microscope objective is required for this configuration.

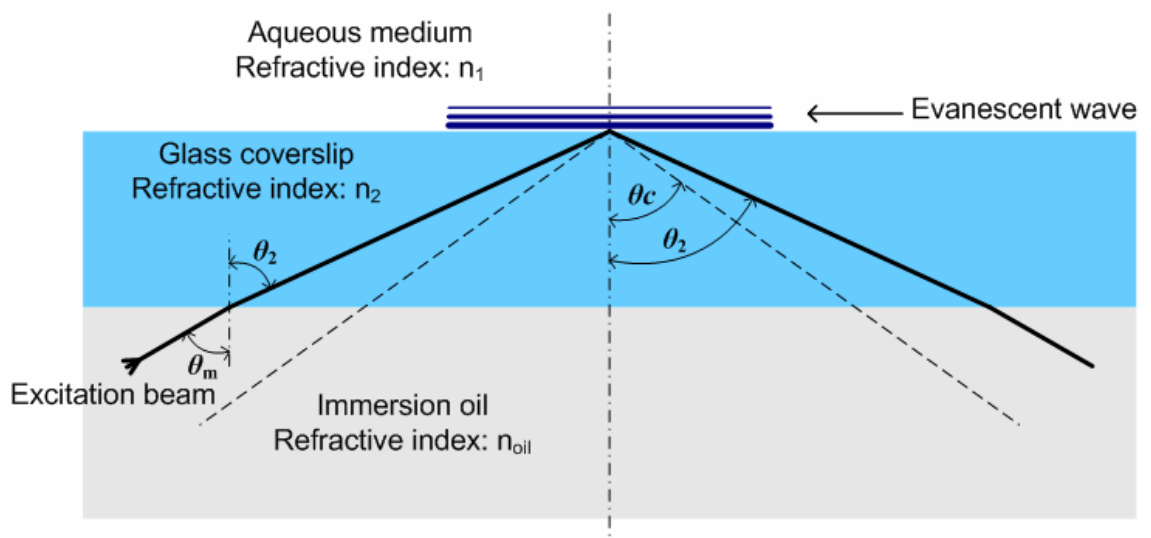


Figure 1.14 High NA objective is needed for prismless TIRF configuration.

Chapter 2 Measurement system and EMCCD camera optimization

The EMCCD camera used in the project is iXon DV-885KSC-VP (Andor Technologies, Belfast, UK.), which is a 14 bit cooled EMCCD. The resolution of the camera is 1004*1002, with 8 μ m*8 μ m pixel size. The camera can be cooled down to -70 degrees when operating and has a maximum QE of about 65% at 600nm wavelength. More detailed specification of this camera can be found on [15]. Although the manufacturer claims that this camera has photon counting sensitivity, it is necessary to assess the camera performance and confirm whether the camera really has the capability of photon counting before the measurement of point spread function.

2.1 Measurement system configuration

To evaluate the performance of the camera, a simple system is built as figure 2.1.

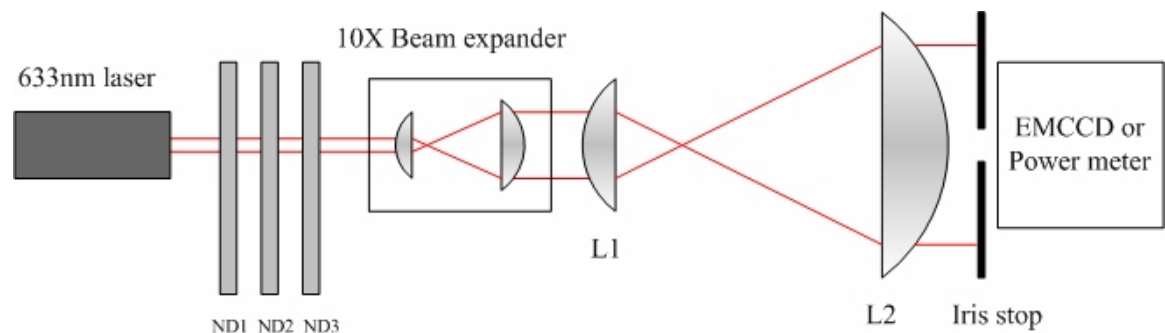


Figure 2.1 schematic diagram of measurement system. Laser source is attenuated by three ND filters, and then expanded by two beam expander with a total 133x magnification.

A 633nm HeNe laser (Power: 20mW, Model: 1135P, JDS Uniphase, CA, USA) is used as light source in the system. The laser beam is expanded by two beam expanders. The first beam expander has a magnification of 10 (LINOS Photonics GmbH & Co. KG, Munich, Germany.), the second one is formed by lens L1 ($f=30\text{mm}$) and L2 (400mm) and the magnification is 13.3. The total magnification is therefore 133 with two beam expander combined.

As the laser profile has a Gaussian distribution, a small central area of the laser beam can be considered as approximately an even distribution after large beam expansion. So we expect to obtain a small area of even illumination (approx $1\text{cm} \times 1\text{cm}$, the size of EMCCD chip) which can be imaged by the EMCCD camera through the iris stop. Because laser is a coherent source, there are many fringes on the image of expanded beam, and a laser beam profiler (LBP-2-USB, Newport Corporation, CA USA.) is

used to find the most evenly illuminated area (figure 2.2). Once the area was determined, the position of the iris stop could be fixed.

In photon counting, even very weak stray light will affect the measurement dramatically, thus the system must be shielded from stray light by blackout material. Since the camera has a build-in shutter, the EMCCD is totally dark when shutter is closed, the stray light shield can be verified by comparing images taken with shutter opened and closed when laser is off. To verify the shielding, the EM gain is set to 200 and exposure time is 1 second, at this setting even an extremely faint light signal will be amplified. Images are taken with shutter opened and closed, we could not observe any difference between the images even we applied statistical analysis such as mean and standard deviation, thus the shielding is confirmed to work well.

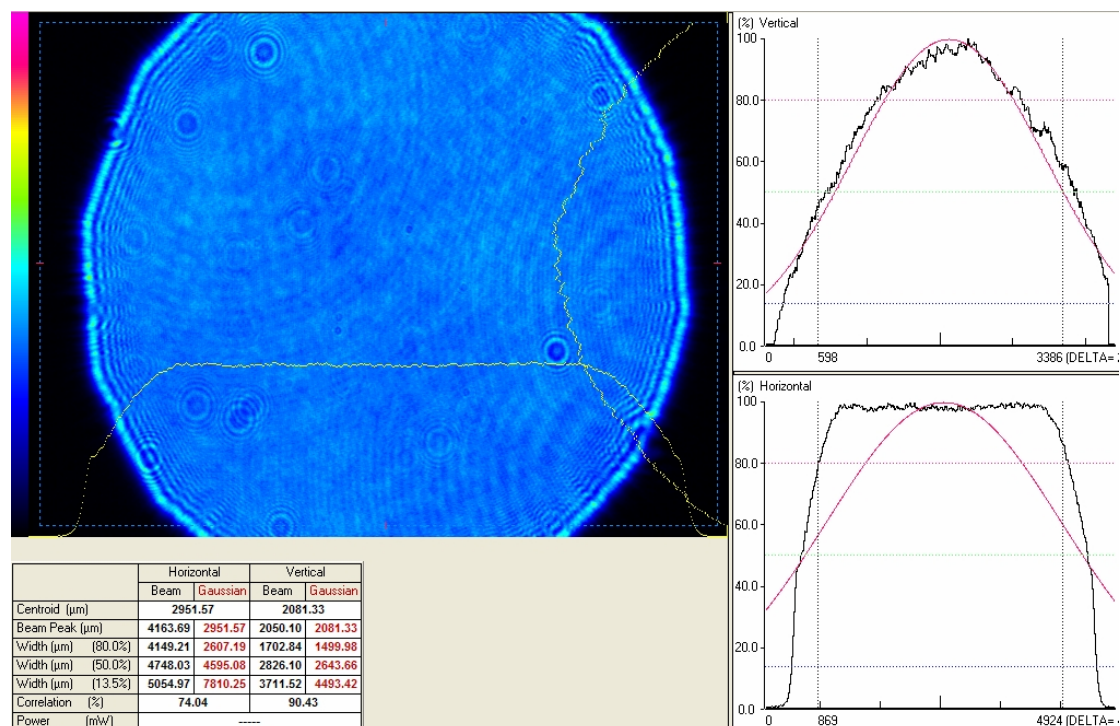


Figure 2.2 Software of laser beam profiler showing the central area profile of expanded laser beam. The image on the left is the beam profile, and the black curves on the right are vertical and horizontal sum profile, each point on the curves represents the sum of the row (or column) pixels at corresponding position. The horizontal profile is almost flat at central area, which means that area is evenly illuminated. Although there are some fringes, the overall intensity can be considered to be approximately evenly distributed. Because of the shape of the beam on the image (the beam profile is not ‘chopped’ at the left and right edge of the image), the vertical profile curve is not flat. The red curves are ideal Gaussian distribution given by the software just for reference.

Three neutral density (ND) filters is used in the system (table 2.1), they can be combined to generate different attenuation factor. The intensity of expanded laser beam and actual attenuation factor of neutral density filters is measured by a power meter (FieldMaxII, Coherent Inc., CA USA.).

Power of expanded laser beam to be imaged by EMCCD (without ND filter attenuation): $0.3\text{mW}/\text{cm}^2$.

	ND1	ND2	ND3
Attenuation factor	77.0	270.4	1936.3

Table 2.1 Attenuation factor of three neutral density filters.

The energy of one photon is given by

$$E = hf = \frac{hc}{\lambda} \quad (2.1)$$

Where h is Planck constant (6.626×10^{-34} Js), f is light frequency, c is light speed, λ is wave length (633nm in this experiment).

The light beam power measured by power meter is 0.3 mW/cm^2 , and the size of pixel on the EMCCD is $8 \mu\text{m}$ by $8 \mu\text{m}$, thus the photon number on each pixel can be calculated.

According to calculation, the attenuation of three neutral density filters, give a light flux arrived at the camera 15.17 photon/pixel/second, take account of the QE of 60%, the effective photon number is 9.10 photon/pixel/second (approximate 9 photon/pixel/second).

2.2 Camera optimization and EM gain calibration

2.2.1 Camera optimization

The image acquisition and camera control software is iQ version 1.5 (Andor technologies.), which provide some adjustable parameters of the camera (figure 2.3).

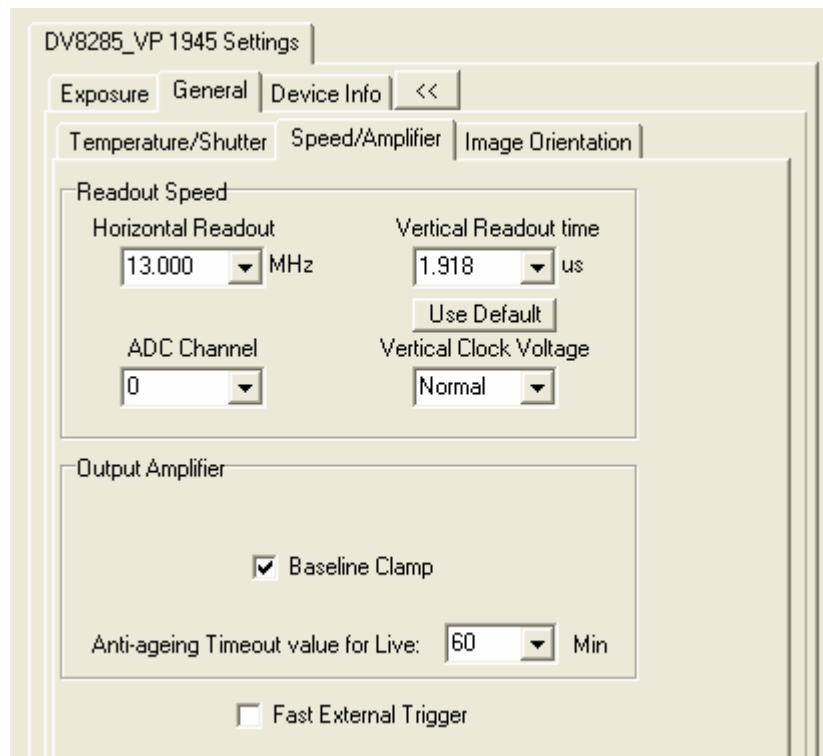


Figure 2.3 Camera setting parameters.

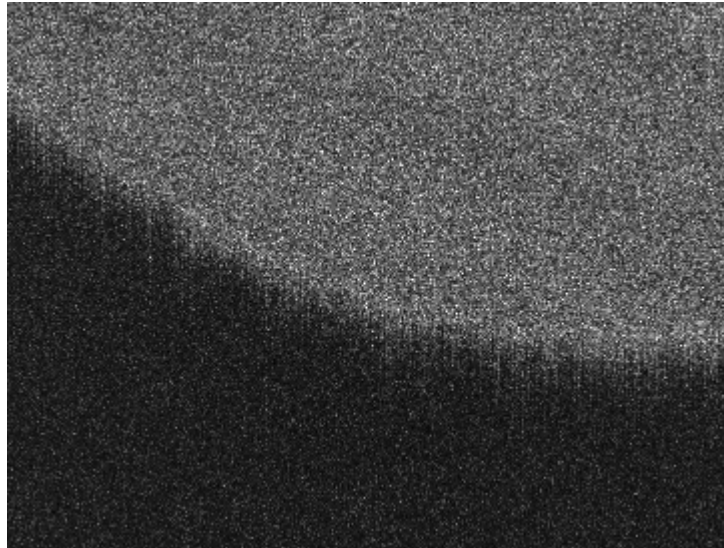
Horizontal readout time determines the collected charge moving speed from horizontal shift register into the output node of the amplifier. As the faster the readout speed the more readout noise is created, this horizontal readout time is set to 13 MHz to keep readout noise low, although a faster speed of 35 MHz is also provided by the camera.

At present time all EMCCDs are of Frame Transfer architecture and require a vertical shift of the image into a storage CCD area prior to readout. The speed and voltage applied during this vertical shift is closely related to CIC level and thus can significantly affect the quality of the image and the background noise level.

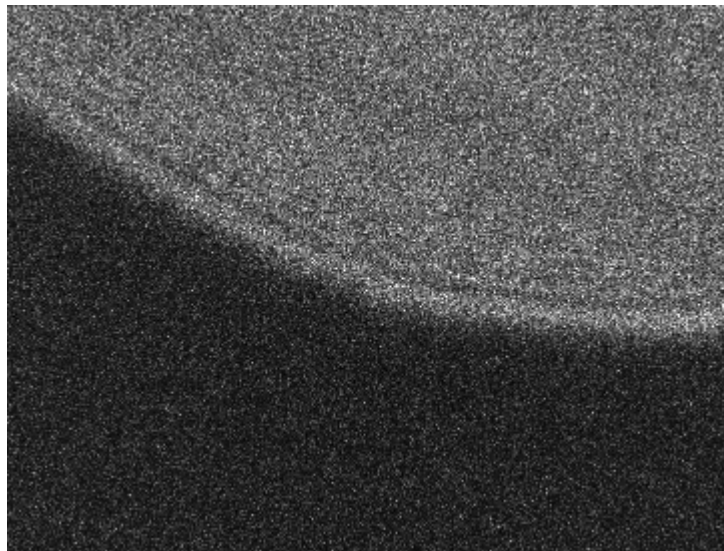
According to the manual of the camera, a faster vertical shift leads to lower background or clock induced charge (CIC) and therefore lower noise. However, faster shift can also lead to lower charge transfer efficiency, which may cause a residual smeared image on the image area.

To overcome this effect the vertical shift voltage can be increased (+1,+2,+3 or +4), but increasing the vertical shift voltage can result in higher CIC level, thus this parameter should be carefully adjusted.

The default settings of these parameter are: vertical shift speed: 1.9 μ s, vertical shift voltage: normal. To reduce noise level, we tried to change vertical shift speed to 0.5 μ s, and the noise level is slightly decreased. However, this resulted in smear image and the image quality is significantly deteriorated, as shown in figure 2.4.



(a)



(b)

Figure 2.4 Image acquired with different vertical shift speed. (a) Vertical shift speed: $0.5 \mu\text{s}$ (smeared image). (b) Vertical shift speed: $1.9 \mu\text{s}$ (normal image).

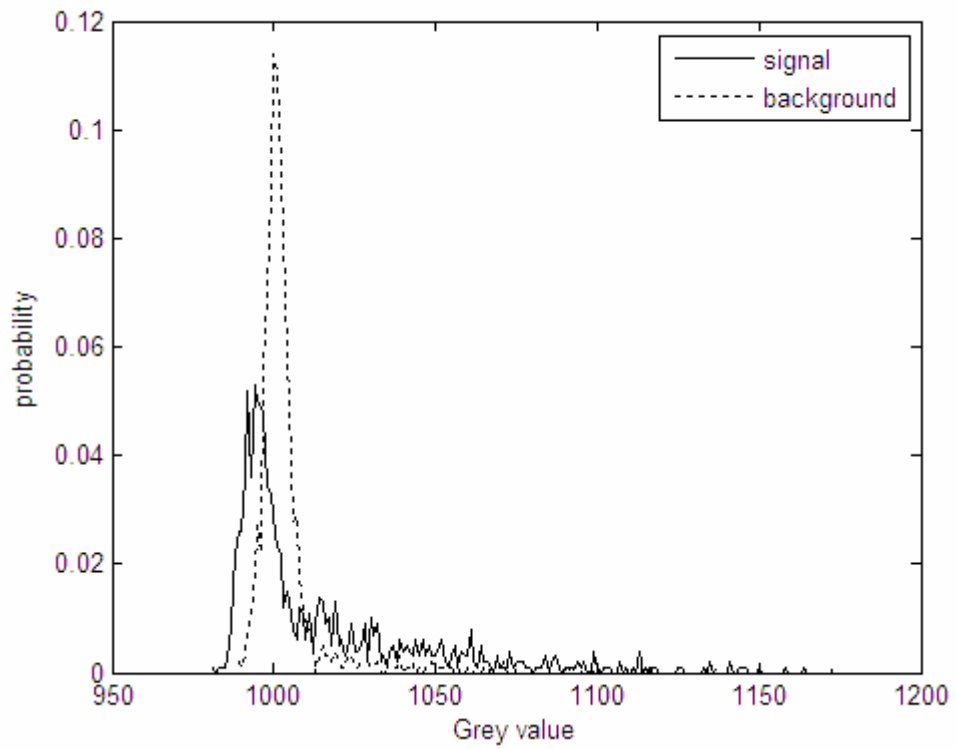
Light flux intensity: 1 photon/pixel/frame, 16 frames averaged. On the pictures, the image with $0.5 \mu\text{s}$ vertical shift speed is smear and all the detail of diffraction fringes is lost.

To overcome this problem, we tried to increase vertical shift voltage, but the noise is increased dramatically when the vertical shift voltage is increased, even at +1. Thus these parameters are restored to default, to keep image quality and relatively low noise.

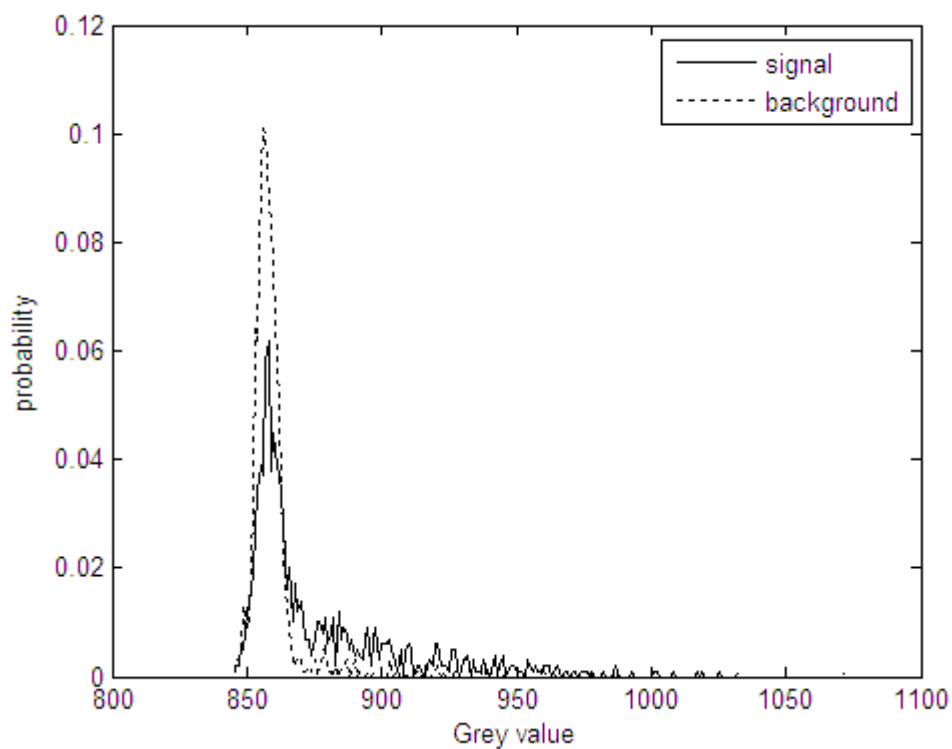
The baseline clamp is another option which may affect the measurement. According to the manual of the camera, the option ensures that the camera electronics adjusts automatically to deliver a baseline count (zero light grey value) at a certain fixed value, so drift in the baseline level caused by small changes in heat generation of the driving electronics can be prevented.

This option is on by default, but I found this option may result in signal level shift for weak signal. Figure 2.5. shows the probability distribution of signal from one pixel with 1 photon/pixel/frame light intensity. As the photon arrival obeys a Poisson distribution, the probability for no photon arrival, one photon arrival and more than one photon are approximate 37%, 37% and 26% respectively. Since the camera is not sensitive enough to detect every 'one photon arrival' event, the peak of signal distribution curve represent the situation that no signal output (i.e. the background), so the peak position in curves of signal and background should coincide. However the peak in signal curve is shifted left with baseline clamp on (figure 2.5 (a)), although the shift is small (about 5-10 count in grey value) and not very significant, it may have some effect on threshold processing in photon counting. This shift does not exist with baseline clamp off, as

shown in figure 2.5 (b), thus the option is turned off in the experiment, although the baseline might drift during experiment with this option off.



(a)



(b)

Figure 2.5 Statistical data of signal of one pixel in a series of 1000 images. Light flux intensity: 1 photon/pixel/frame. (a) Baseline clamp ON. (b) Baseline clamp OFF.

2.2.2 EM gain calibration

The EM gain can be controlled by the software. However, the gain value in the software is not linearly proportional to the real EM gain of this camera, although some newer models of EMCCD cameras provide linear gain setting. Thus gain calibration for the camera is needed. To calibrate EM gain, an object with constant light intensity is imaged on the camera,

several pictures are taken at different EM gain settings, and the grey value subtracted by background is proportional to real gain. As the camera is a 14 bit EMCCD, the grey value on image ranges from 0 to 16383, and the EM gain can be up to more than 1000, the camera can be saturated at high gain. Thus exposure time must be reduced at high gain setting, and the exposure time ratio need to be take into account when calculating real gain.

Software gain	Real gain
OFF	1
1	2.4
50	4.5
100	12.1
150	55.4
175	149
185	235
200	481
210	776
220	1308
230	2500

Table 2.2 Relationship between real gain and software gain setting.

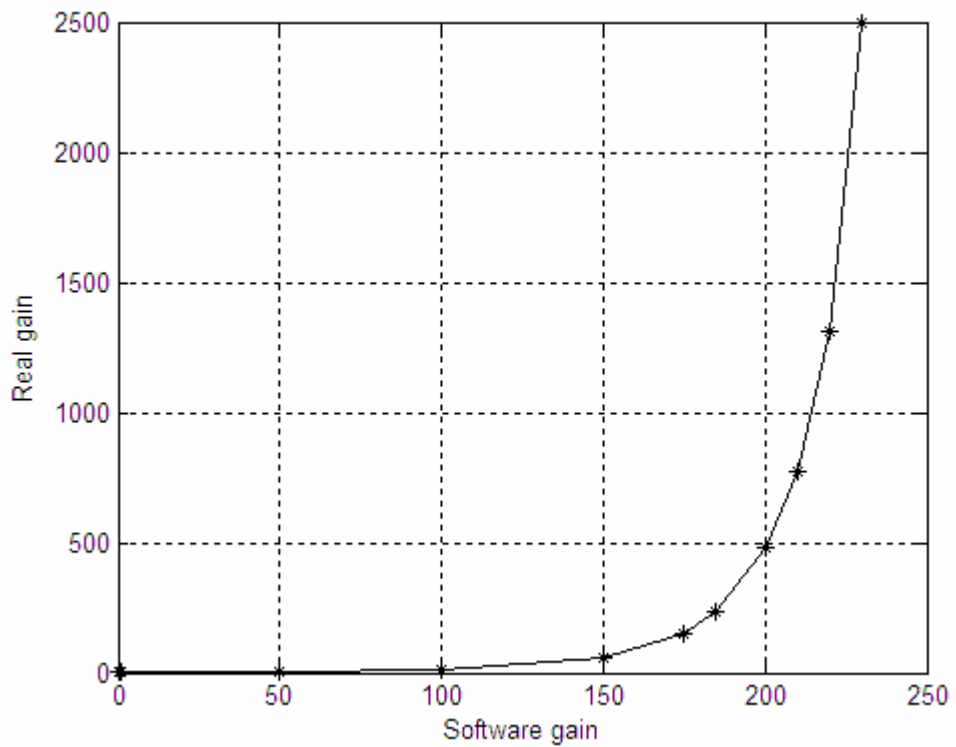


Figure 2.6 Plot of software gain setting versus real gain value

2.2.3 Choosing a suitable EM gain value

Although signal is amplified greatly at high EM gain, the noise is also increased significantly at the same time. The EM gain value need to be carefully choose to achieve optimized signal to noise ratio. The background noise is measured by calculating standard deviation of totally dark image of different gain value. We define the ratio real gain / background standard deviation as the 'signal to noise ratio' in the experiment. The ratio is calculated for different gain and the most suitable gain value can be obtained.

Software gain	Real gain	Background standard deviation	Real gain/std dev.
OFF	1	3.6	0.28
1	2.4	3.7	0.65
50	4.5	3.7	1.22
100	12.1	3.8	3.21
150	55.4	6.1	9.07
175	149	12.6	11.8
185	235	20.0	11.7
200	481	41.0	11.7
210	776	68.6	11.3
220	1308	119.1	11.0

Table 2.3 Relationship between software gain and ratio of real gain/background standard deviation

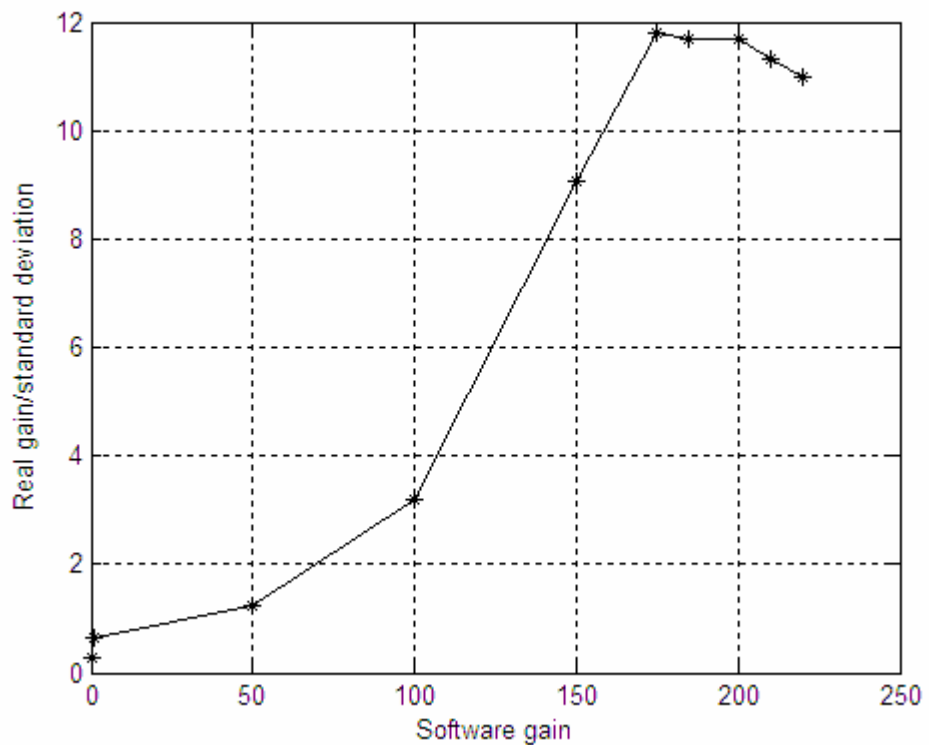


Figure 2.7 Plot of software gain versus ratio of real gain/background standard deviation

According to table 2.3 and figure 2.7, at low gain value the ratio 'real gain/background standard deviation' increases rapidly with gain, which means the gain has significant effect on improving signal to noise ratio. The ratio reaches its peak at gain 175 and almost keep constant till gain 200, then it began to decrease when gain is greater than 200, which is due to the dramatically increase of noise, so the effective signal to noise ratio will not get improvement, or even get worse as gain go beyond 200. Thus the gain value of 175 is considered as the most suitable gain value for the experiment.

Chapter 3 Evaluating photon counting performance of EMCCD

3.1 Principle of photon counting by EMCCD

Since the EM amplification that is applied in the gain register is a stochastic process, although probability distribution can be calculated (figure 1.13), the exact input photon number cannot be deduced by the magnitude of output signal.

To perform photon counting, the light intensity must be kept at a very low level so it can be assumed that either only one photon, or no photon arrive at one pixel during one exposure. Under this condition, a threshold is set and all signals above the threshold will be counted as signal of one photon, the signals below the threshold will be considered as dark.

The arrival photon number obeys Poisson distribution, which is given by

$$p(n, I) = \frac{I^n \exp - I}{n!} \quad (3.1)$$

Where $p(n, \lambda)$ is the probability of n events occurring when the averages (expectation number) is λ .

Table 3.1 gives some probability with different λ (mean value).

Mean (λ)	0.05	0.1	0.2	0.5	1	2	5
P(n=0)	0.95123	0.90484	0.81873	0.60653	0.36788	0.135335	0.006738
P(n=1)	0.047561	0.090484	0.16375	0.30327	0.36788	0.270671	0.03369
P(n=2)	0.001189	0.004524	0.016375	0.075816	0.18394	0.270671	0.084224
P(n=3)	1.98E-05	0.000151	0.001092	0.012636	0.061313	0.180447	0.140374
P(n>1)	0.001209	0.004679	0.017523	0.090204	0.26424	0.593994	0.959572
Ratio P(n=1)/P(n>1)	39.336	19.339	9.3446	3.362	1.3922	0.455679	0.035109

Table 3.1 Poisson distribution probability with different λ .

As the light intensity measured above is the average intensity, for example at light flux 1 photon/pixel/exposure, there is still a relative high probability $P(n>1)=0.26424$ of having more than one photon in a exposure, the light intensity should be kept very low to satisfy the condition ‘either only one photon, or no photon arrives during one exposure’. At light intensity 0.1 photon/pixel/exposure, the probability of having more than one photon $P(n>1)=0.004679$ is very small and can be considered to be negligible.

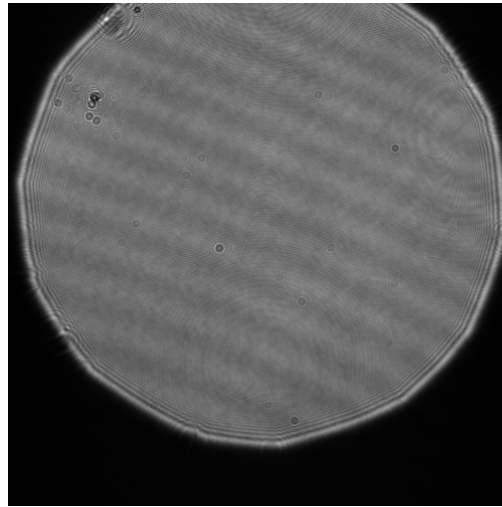
3.2 Method

Although the light intensity is measured by power meter, there are some fringes on the laser beam, and not every pixel illuminated by laser beam has the same intensity. Since the light intensity measured by the power meter is the average power over the area, so we need to choose pixels

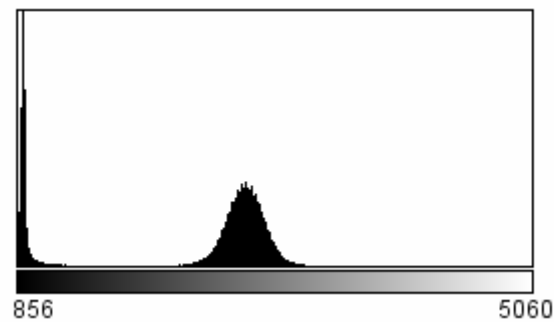
having light intensity corresponding to the intensity measured by power meter.

Firstly ND1 and ND2 are removed so the intensity is high enough for normal CCD imaging, the EM gain in the camera is also turned off. Then an image is taken by the camera and the histogram is obtained, as shown in figure 3.1. The image on figure 3.1(a) has some fringes, the grey value difference between peak and lowest position is about 15% of the average value of the entity illuminated area. On figure 3.1(b) the left peak on the histogram represents dark pixels without illumination, the central symmetrical distribution represents the pixels illuminated by the laser beam. The average power of the illuminated area is obtained by the power meter, which corresponds to the central position of the distribution on the histogram. The grey value at central position is recorded and the pixels with the same grey value have the same intensity with average power of the area.

According to the power meter measurement, the output power of laser is not perfectly constant, the fluctuation is approximate 5%. The attenuation factors of ND filters, although calibrated by the power meter, still have an error of approximate 2~3% each, it is estimated the error is approximately 5% ($\sqrt{3 \times 0.03^2}$) when three ND filters combined. Therefore the total error of photon number arrival at the camera is approximate 7% ($\sqrt{0.05^2 + 0.05^2}$).



(a)



(b)

Figure 3.1 (a) Image of laser beam without ND1 and ND2. (b) Histogram of the image.

After choosing pixels, ND1 and ND2 are restored and EM gain in the camera is set to 175, the exposure time is set as corresponding required mean photon number (light intensity). For example, the laser beam intensity is 9 photon/pixel/second, a exposure time of 111 millisecond is needed to achieve the intensity of 1 photon/pixel/exposure, and 11 millisecond for 0.1 photon/pixel/exposure and so on. The exposure is set as repeating up to 50,000 times automatically, so a stack of images can be

obtained. To save storage space and increase acquisition speed, only a small area of 80*80 pixels is recorded. For each light intensity level, two stacks of images are acquired, one with camera shutter opened represents signal, and one with shutter closed represents background noise.

3.3 Result and data analysis

3.3.1 Probability density distribution

For each pixel chosen previously, the pixel grey value is read from the image stacks, so a series of grey value data is obtained for one pixel. These data is processed by statistical analysis, and the mean, standard deviation and probability distribution are obtained. Table 3.2 shows the statistical data of a pixel signal, for light intensity 0.1 and 0.2 photon/pixel/exposure, 50,000 exposures are acquired, and for light intensity 1 photon/pixel/exposure, 10,000 exposures are acquired. Figure 3.2, 3.3 and 3.4 shows the probability density distribution (probability density function, PDF) of the pixel signal response with different illumination light intensity.

Light intensity (photon/pixel/exposure)	0.1	0.2	1
Signal mean	879.15	876.24	886.4
Background mean	876.63	873.81	872.08
Signal std. deviation	16.965	19.012	32.622
Background std. deviation	13.324	13.624	13.791

Table 3.2 Mean and standard deviation of signal and background at different light intensity.

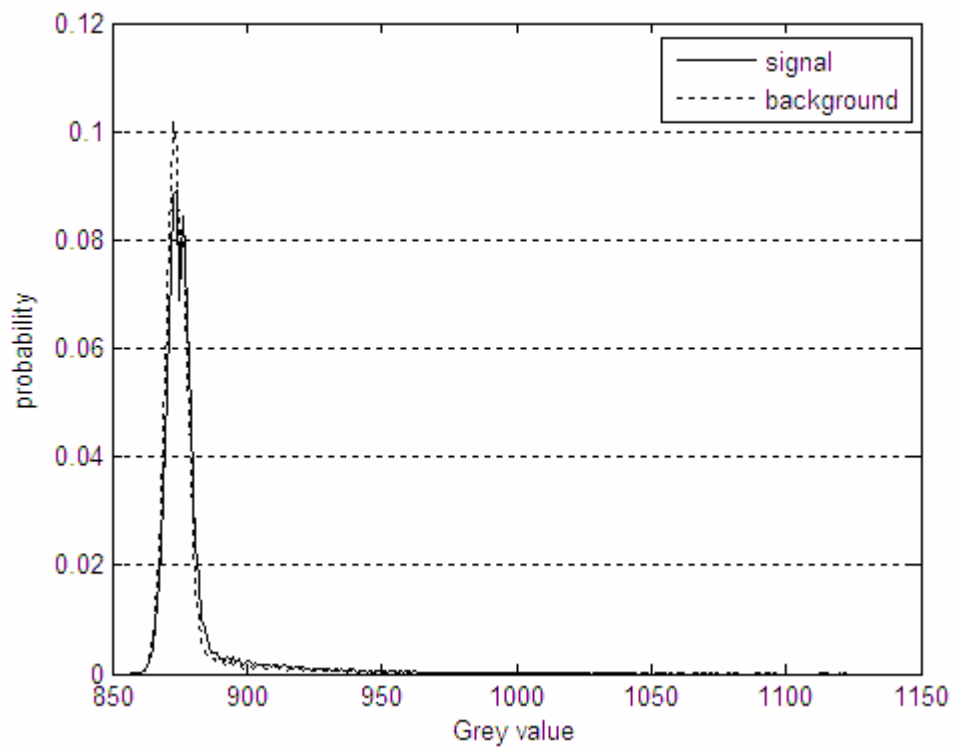


Figure 3.2 Probability density distribution of one pixel signal from a series of 50,000 images, illumination light intensity 0.1 photon/pixel/exposure.

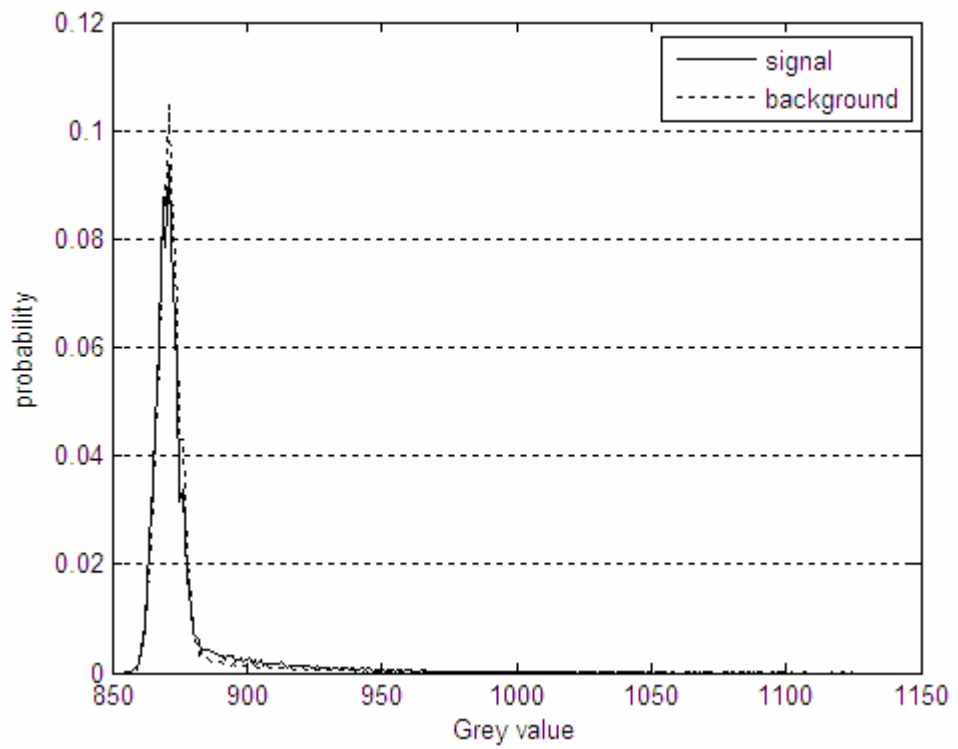


Figure 3.3 Probability density distribution of one pixel signal from a series of 50,000 images, illumination light intensity 0.2 photon/pixel/exposure.

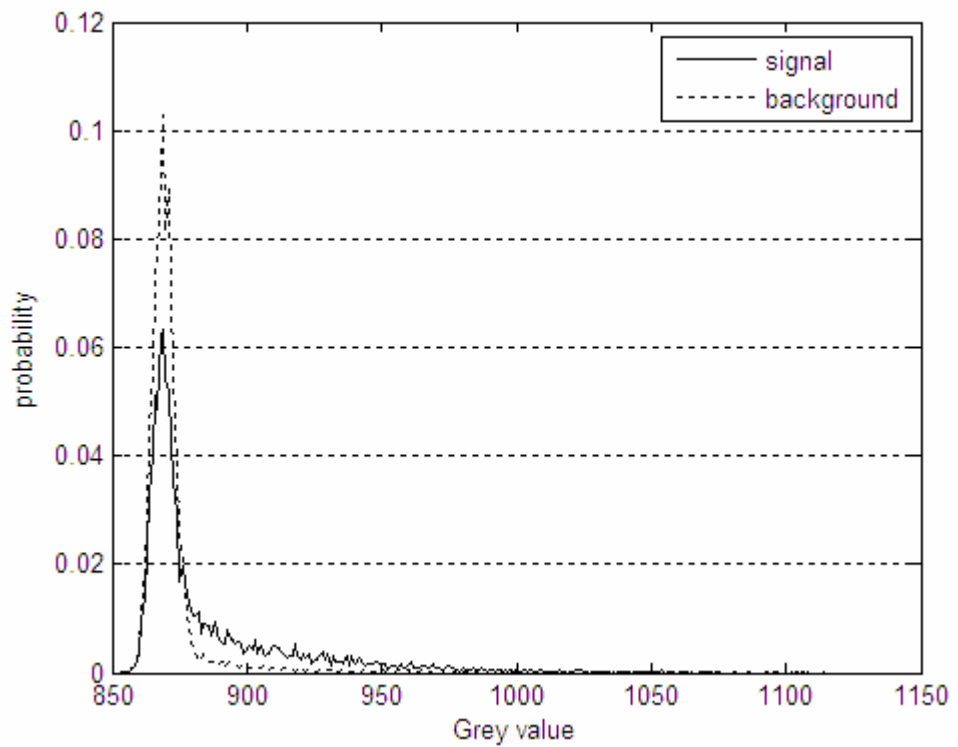


Figure 3.4 Probability density distribution of one pixel signal from a series of 10,000 images, illumination light intensity 1 photon/pixel/exposure.

According to the figures above, the signal and background distribution is very close at intensity 0.1 or 0.2 photon/pixel/exposure, it is because most exposures are dark at low intensity, for example, at intensity 0.1 photon/pixel/exposure approximately 10% of total exposures receive a photon, and 90% exposures are dark without photon.

At intensity 1 photon/pixel/exposure the signal and background distribution are more separated, the signal has higher probability at high grey value. However, according Poisson distribution, at this intensity the probability of having more than one photon arrival during one exposure is about 26.4%, and if photon counting is performed at this intensity, all situations with more than one photon will be counted as one photon.

The background distribution has a peak (around grey value 870), which represents the baseline (zero light grey value) of the camera. The background probability decrease dramatically as grey value increases, but it does not drop to zero immediately, above grey value 880~890 the probability decreases more slowly and can spread widely up to around 1000. Thus the distribution of background and signal overlap, this overlapping causes a problem on photon counting. As described previously a threshold is needed in photon counting, the widespread distribution of background make it difficult to set the value of threshold. If the threshold is set low, the noise or false counting will be very high, on the other hand, if the threshold is set as high, the noise can be eliminated but most signal is excluded at the same time. This problem is especially significant at low

light intensity, as the distribution of signal and background are very close, unfortunately the photon counting requires low light intensity to satisfy the condition 'no more than one photon arrives during one exposure'. Thus the background noise level of the EMCCD camera determines whether photon counting is feasible.

3.3.2 Cumulative distribution

To research the performance of the camera, a cumulative distribution function (CDF) is calculated from corresponding probability density distribution. The cumulative distribution function is obtained by setting a variable 'value' and calculating the probability that $x \geq$ 'value' from probability density distribution, and this probability is plot against 'value'.

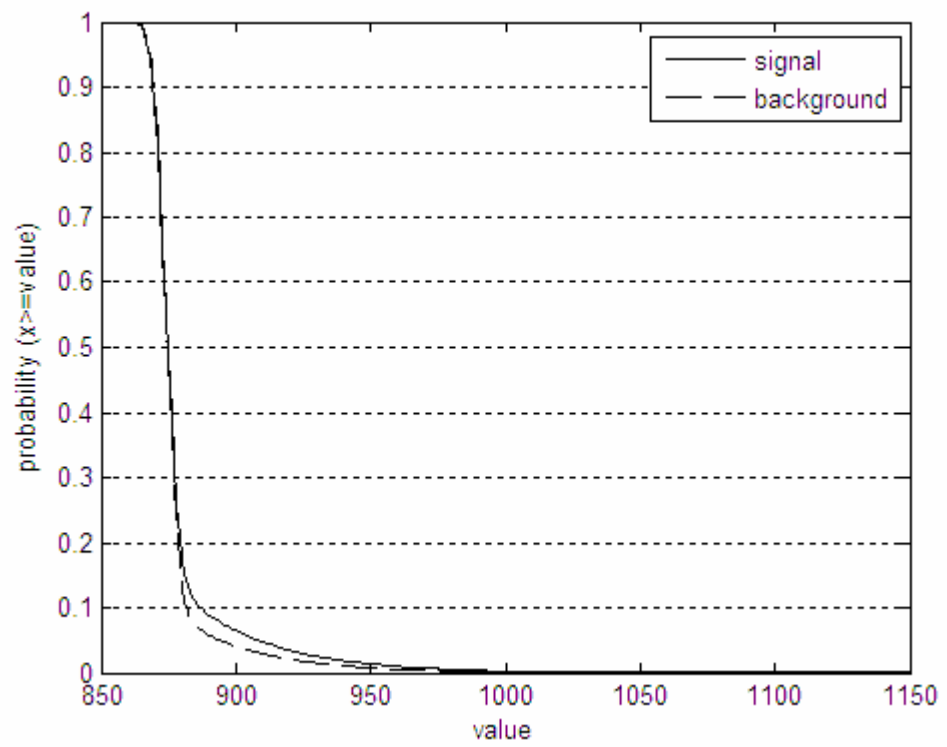


Figure 3.5 Cumulative distribution function of one pixel signal from a series of 50,000 images, illumination light intensity 0.1 photon/pixel/exposure.

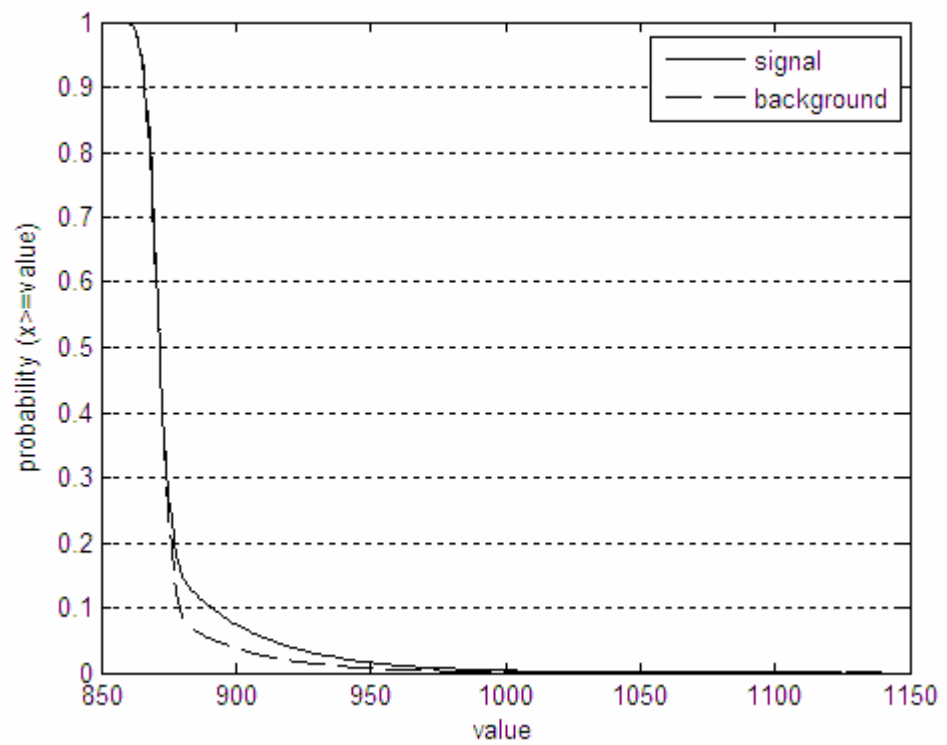


Figure 3.6 Cumulative distribution function of one pixel signal from a series of 50,000 images, illumination light intensity 0.2 photon/pixel/exposure.

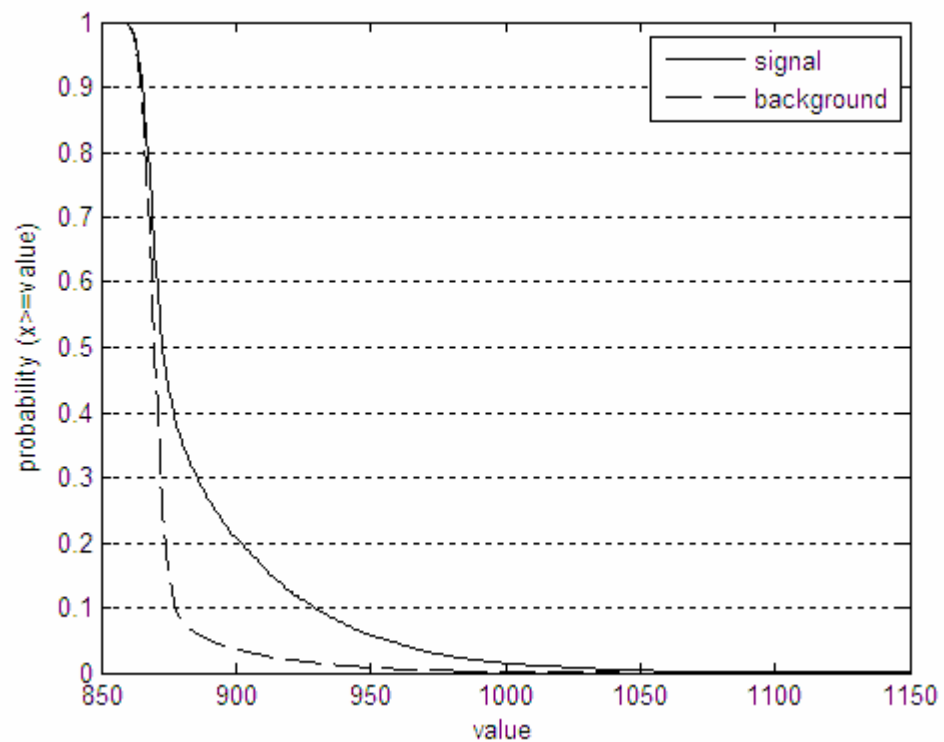


Figure 3.7 Cumulative distribution function of one pixel signal from a series of 50,000 images, illumination light intensity 1 photon/pixel/exposure.

The cumulative distribution functions give the probability that signal or background is greater than a certain threshold value at different photon mean number, so the proper threshold value can be determined from these cumulative distribution functions.

At low light intensity, the probability that of signal does not exceed that of background too much no matter what threshold value is chosen (figure 3.5 and 3.6), which is caused by the widely spread distribution of background and the overlap of background and signal distribution as described above. As a result, the signal to noise ratio is low at low light intensity. For example, at intensity 0.1 photon/pixel/exposure, if value 900 is chosen as

threshold, the probability of signal is about 0.067, and probability of background is about 0.041. As the signal obtained from camera also includes background noise, more than half of the counts will be noise if photon counting is performed at this intensity with threshold value 900.

At higher light intensity, the probability of signal and background are better separated (figure 3.7) so the signal to noise ratio is higher. On the figure, the ratio 'signal : background' could be higher if the threshold is set at a higher value, as the background is reduced to very low, however it is not feasible in practice.

If the threshold is set too high, most signals will be excluded and only strong signals can remain, since the arrival of a photon obeys the Poisson distribution, at intensity 1 photon/pixel/exposure there is still a non-negligible probability of more than one photon (about 26.4%). According to probability distribution of EMCCD output charge (figure 1.13), the more input electron the higher probability of having a larger number output charge and therefore a stronger signal. In this case, the signals remained after threshold processing is more likely to be due to the situation of two or more photons rather than one, so the signal might not represent one photon and it could result in error in photon counting. Moreover, since most signals are excluded after threshold processing, the effective detection efficiency will be very low, so more exposures are needed to acquire enough signals, and more acquisition time and storage space is needed.

3.3.3 Estimation of the CDF of one photon

According to table 3.1, at mean 0.1, the probability $P(n>1)$ is very small so it can be neglected, so $P(n=1)$ can be approximated by $P(n>0)$, thus $P(n=0)$ and $P(n=1)$ are approximate 0.905 and 0.095 respectively. The CDF(0.1) in figure 4.5 can be considered as:

$$CDF(0.1) = 0.905CDF(0) + 0.095CDF(1) \quad (3.2)$$

Where $CDF(0.1)$ is it is the CDF of signal in figure 3.5, $CDF(0)$ is cumulative distribution function of pixel signal when there is no photon incident, it is the CDF of background in figure 3.5. $CDF(1)$ is cumulative distribution function of pixel signal when there is one and only one photon incident, it can be calculated from equation 3.2. Figure 3.8 shows the calculated $CDF(1)$ from figure 3.5.

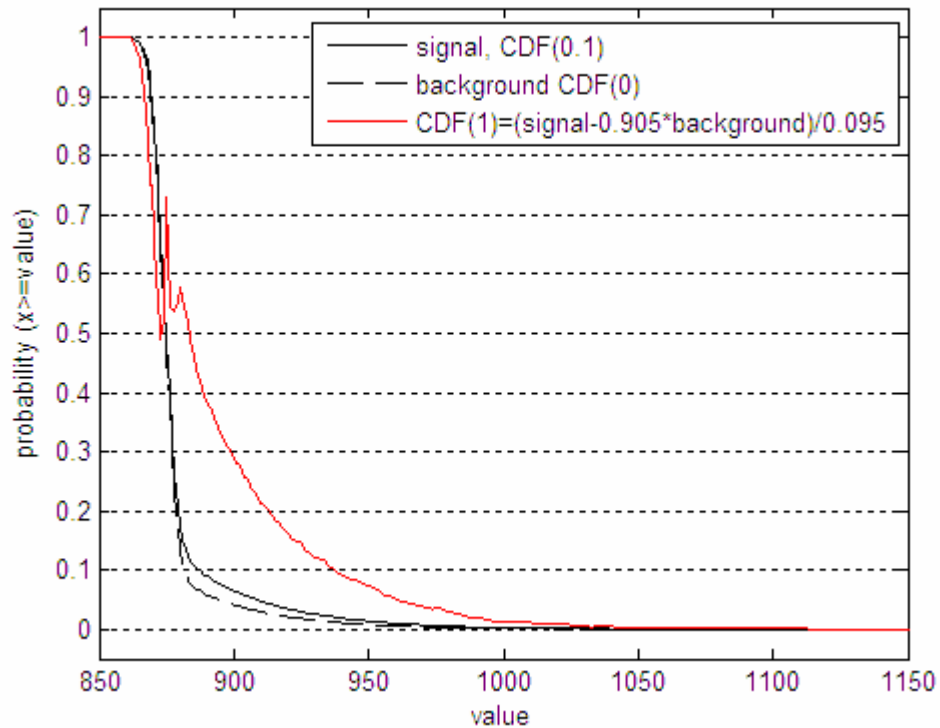


Figure 3.8, Curve of calculated CDF(1) of the pixel on figure 4.5 by $(CDF(0.1) - 0.905CDF(0))/0.095$. The CDF of signal and background (black solid and black dashed line) are same as that in figure 3.5.

The calculated CDF(1) in figure 3.8 has some peaks near value 870 where the curve of signal and background are steep. The curve of CDF should not have peaks in real situation, as the cumulative distribution function is always monotonically decrease by its definition, peaks in CDF means negative probability in the regions which is not possible in real world. The peak in the calculated CDF(1) is possibly due to measurement error, a very small different between signal and background in the steep region will be significant, since the option baseline clamp is off, the baseline level might drift slightly during the experiment, which might result in the peaks in the curve. Therefore the data in the steep region is not reliable and will not be

used. Table 3.2 shows the probability of signal of 1 photon and background at several different threshold values.

Threshold value	Background probability	Signal of 1 photon probability
882	9.33%	53.04%
894	5.03%	34.57%
942	0.99%	8.86%
963	0.5%	4.58%

Table 3.2 Probability value of CDF(0) and CDF(1) in figure 3.8 at different threshold value.

3.3.4 Simulation of signal distribution

The signal and background distribution can be calculated by a simulation model. Let the probability of detecting a photon when it is actually there be p_d , the probability of a false positive (the signal when there is no photon) be p_f . The expected photon number at the pixel is f , where the number f should be much less than 1, and a total image number of N is taken in the measurement.

Thus within a single frame the probability of detecting a photon when it is actually present is:

$$p_d' = (1 - p(f,0))p_d \quad (3.3)$$

Where the function $p(a,b)$ is the Poisson function for expectation value a and value b , the number f should be much less than 1, so $P(n=1)$ can be approximated by $P(n>0)$.

The probability of false positive:

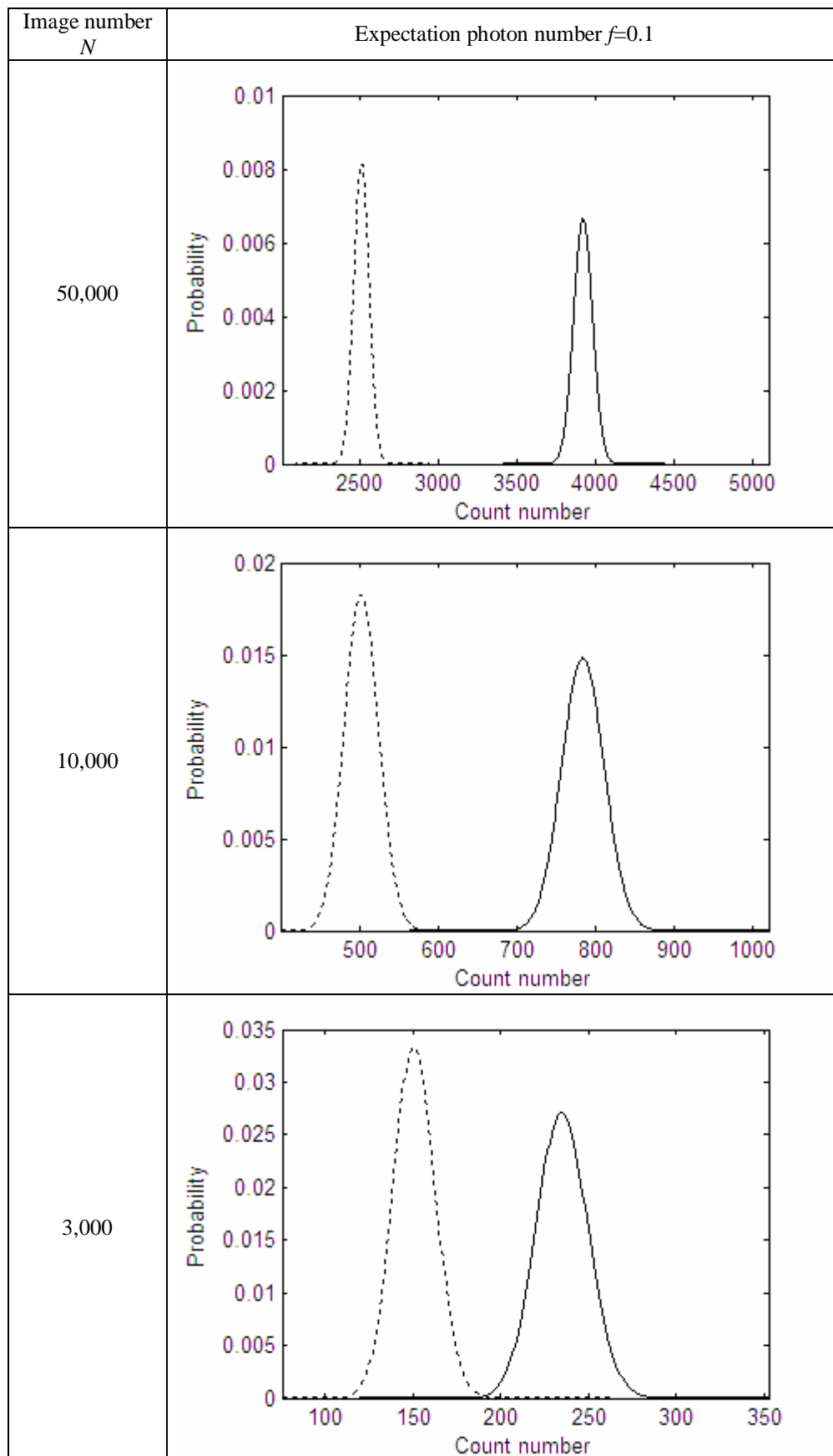
$$p_f' = p(f,0)p_f \quad (3.4)$$

The probability of detector output p will be p_f' when it is in totally dark.

If there is photon incident, the total signal probability of detector output with background will be

$$p = p_d' + p_f' \quad (3.5)$$

So the distribution can be calculated by Binomial distribution for different values of p_d , p_f , f and N . For example using data $p_d = 34.57\%$, $p_f = 5.03\%$ in table 3.2, the signal and background probability distributions at different f and N are obtained by MATLAB simulation in figure 3.9 and 3.10.



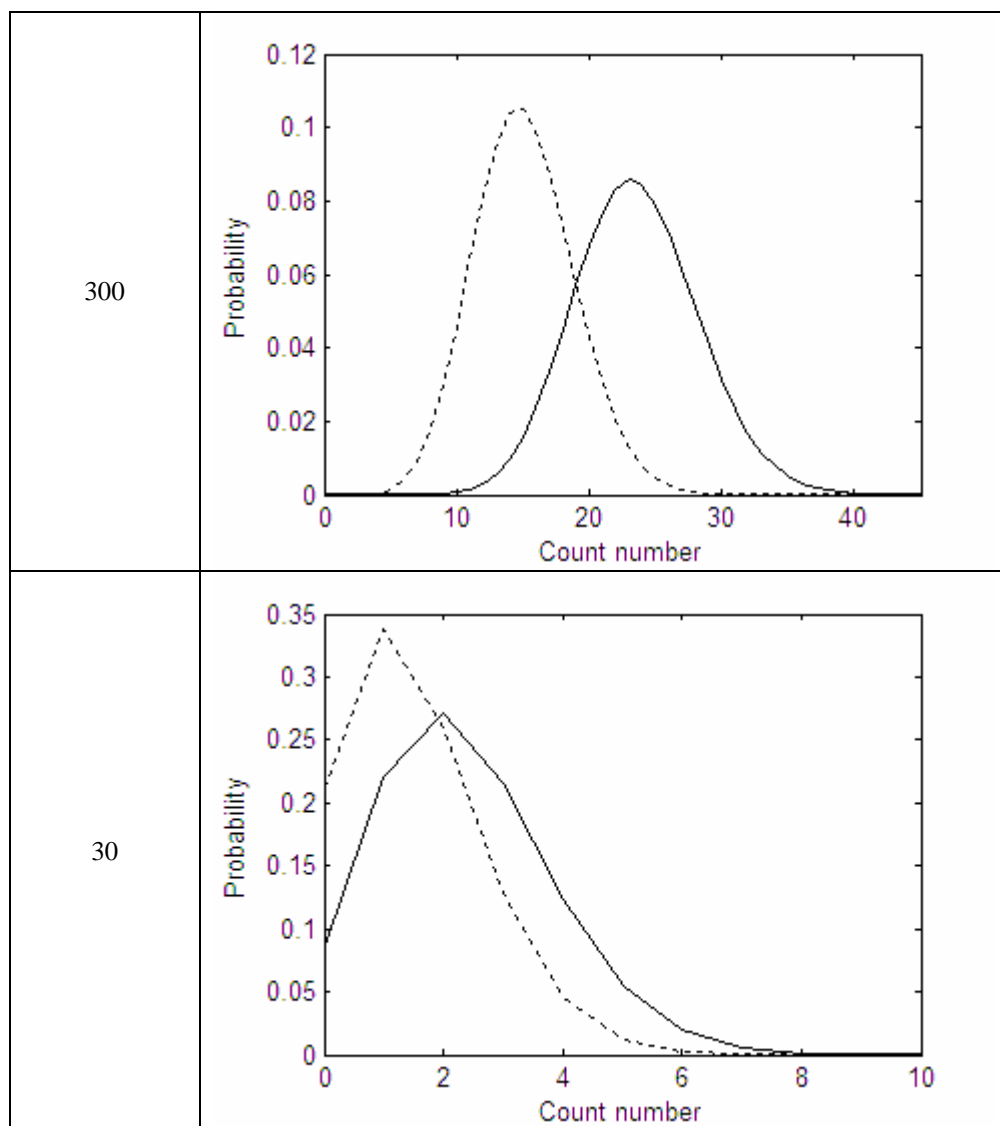
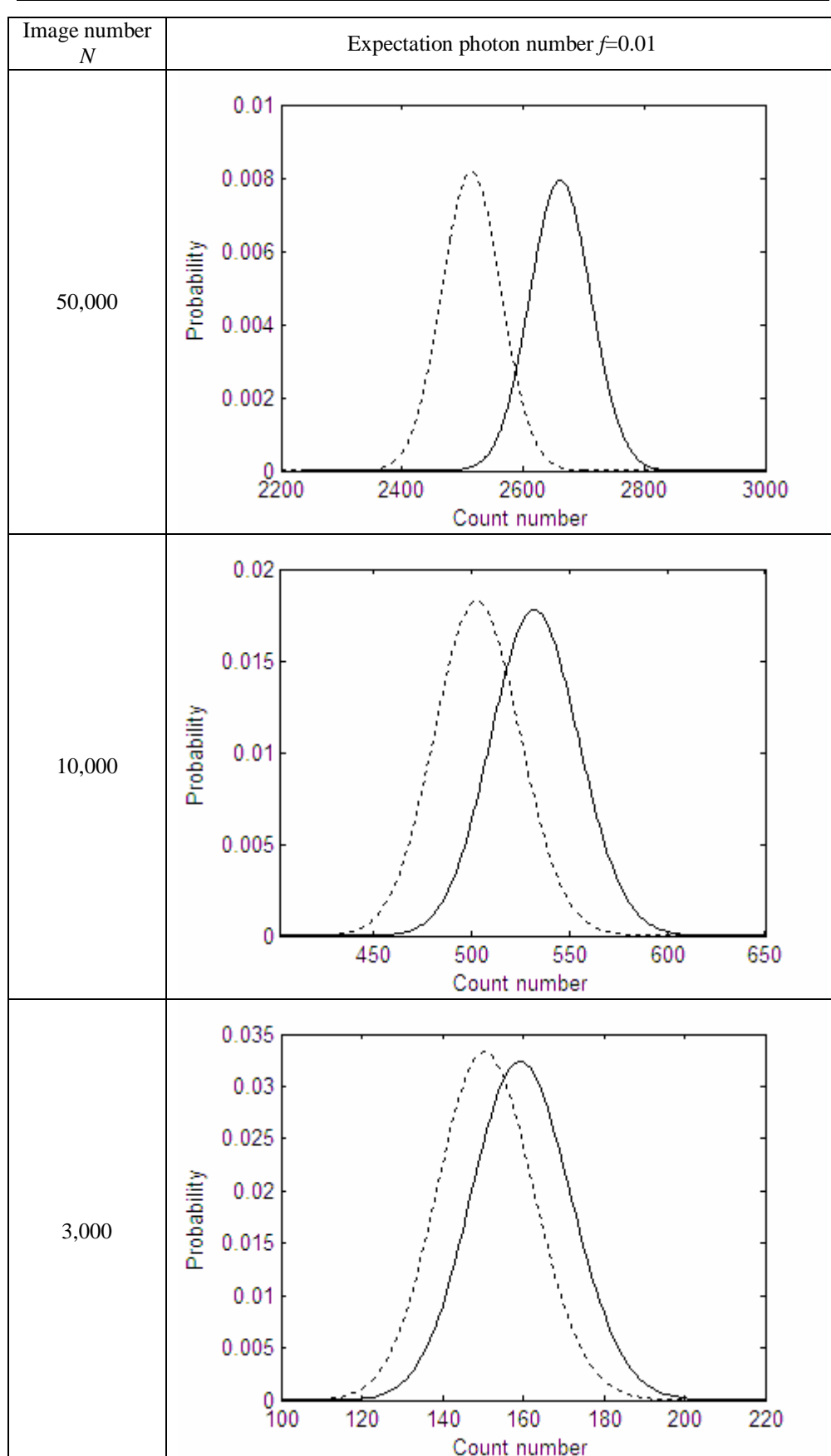


Figure 3.9, Simulation of signal and background distribution at different image number N for $f=0.1$, $p_d = 34.57\%$, $p_f = 5.03\%$. The solid line represents signal with background, and the dotted line represents background.



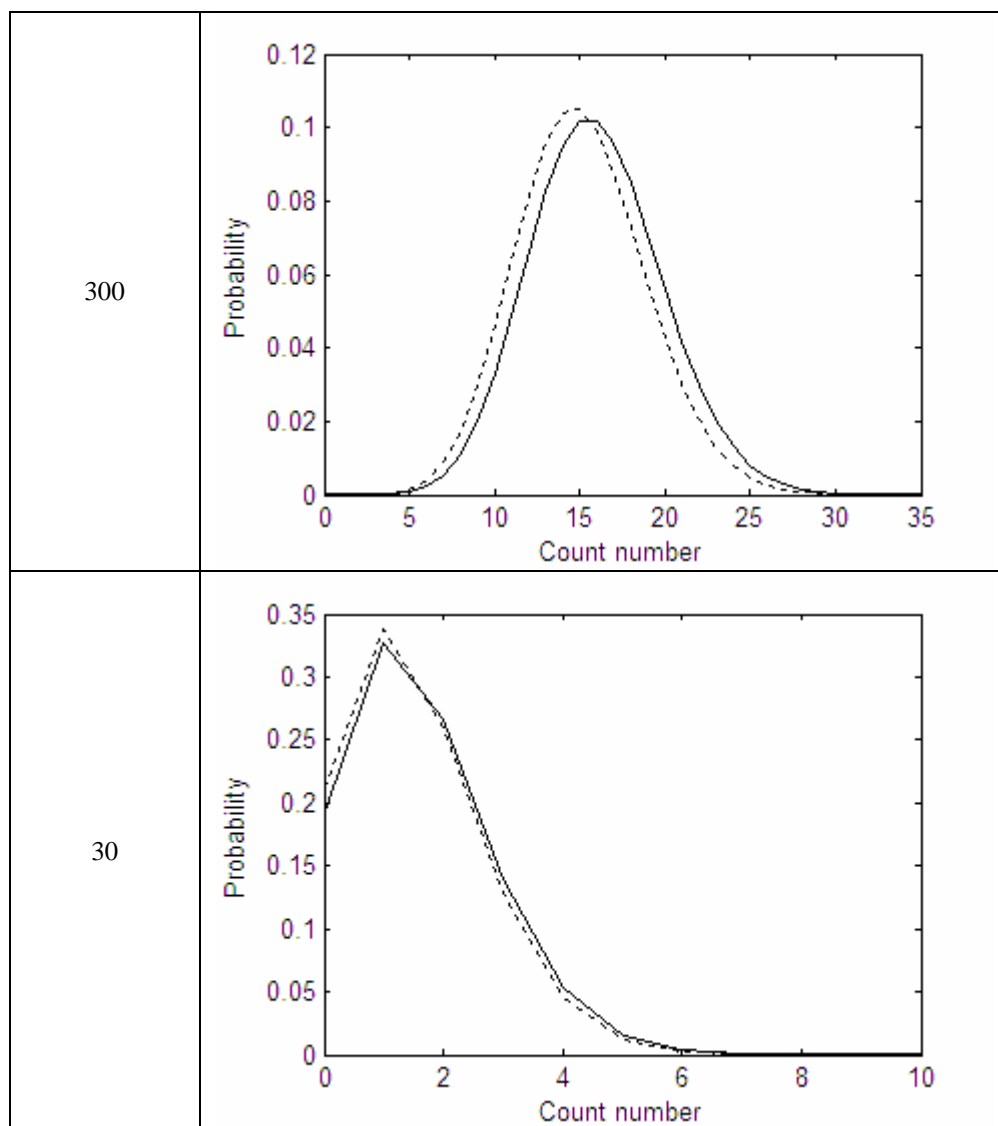


Figure 3.10, Simulation of signal and background distribution at different image number N for $f=0.01$, $p_d = 34.57\%$, $p_f = 5.03\%$. The solid line represents signal with background, and the dotted line represents background.

According to figure 3.9 and 3.10, the distribution of signal and background are well separated at high N and f value. As expected although signal can be separated from background, the exact signal count in practical measurement cannot be obtained simply by subtracting background mean

value from signal, because the background noise is distributed in a region and the exact noise included in the output signal is unknown.

The distributions become closer and overlap when N decrease, for example, at $f=0.1$, the distributions begin to overlap when N is less than 3000. At $N=30$, where the total expectation photon number is approximate 1 ($0.1 \times 34.57\% \times 30 = 1.0371$), most of the two distributions overlap and it is very difficult to distinguish signal from background under this condition. Therefore the camera might not be ideal for photon counting.

The distributions also become closer and overlap with the decrease of f number, it can be observed that at $f=0.01$ the distribution overlap even at $N=50,000$. At the same total expectation photon number, the distribution with lower f number is more overlapped than that of higher f number, as shown in figure 3.11. Thus it is more difficult for the camera to distinguish signal from background at lower light level.

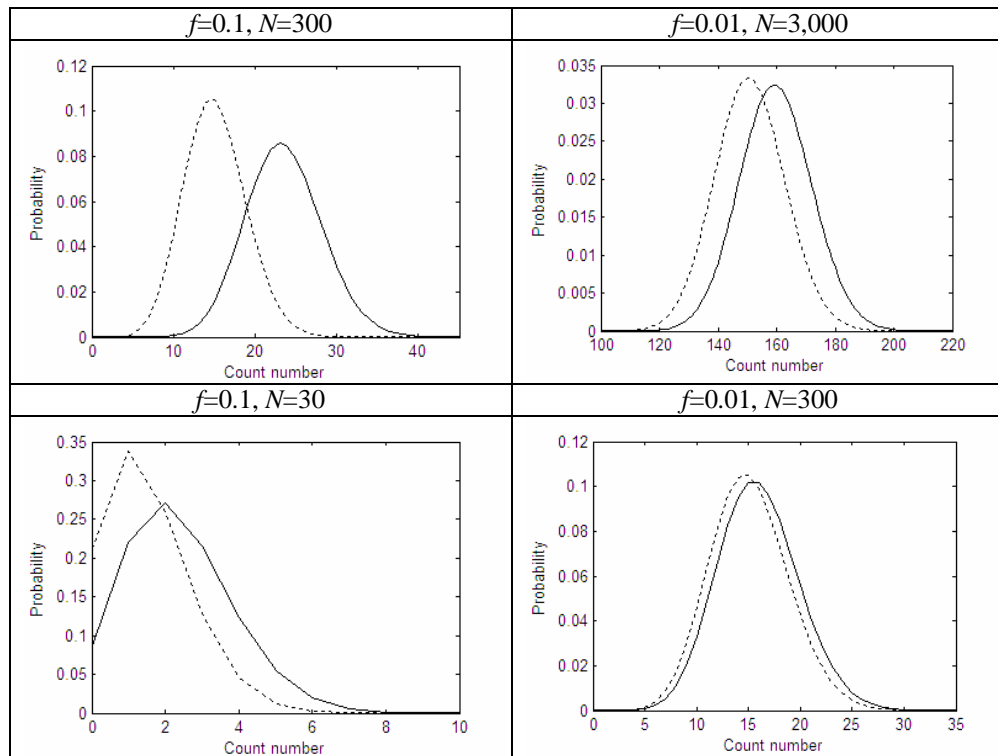


Figure 3.11 Comparison of distribution at different expected photon number f under the same total expectation photon number. The solid line represents signal with background, and the dotted line represents background.

For a point spread function which can be described by a jinc function, the intensity profile is the square of jinc function, and the intensity of first sidelobe is only approximate 1.75% of the peak intensity. According to the simulation result, it will be almost impossible to distinguish sidelobe of point spread function in photon counting with the parameters used for the present camera.

3.3.5 Conclusion

According to the experiment data and simulation result above, although the camera is able to separate signal from background when expectation photon number f and image number N is relative high (for example, $f=0.1$ and $N=10,000$), the exact signal count cannot be obtained because of the variance of background.

When the expectation photon number f decreases, the situation become worse, the distributions of signal and background overlap. Thus the region of point spread function with lower intensity (for example, the sidelobe of PSF) will be merged by background and cannot be detected.

The value p_d and p_f determines the performance of the detector, for an ideal detector $p_d = 1$ and $p_f = 0$. However the practical detector cannot be so good, for example the practical value $p_d = 34.57\%$, $p_f = 5.03\%$ are used in the simulation above. The value of p_f can also be calculated for a 'good performance' detector, for example, under the condition $p_d = 34.57\%$, $f=0.1$, $N=30$ where the total expectation photon number is approximate 1, p_f need to be less than approximate 0.2% to well separate signal and background (figure 3.12). It can also be observed that to achieve a good performance at a lower f number, an even lower p_f is needed.

The camera used in the experiment has a relative high value of p_f , thus it is not very ideal for photon counting.

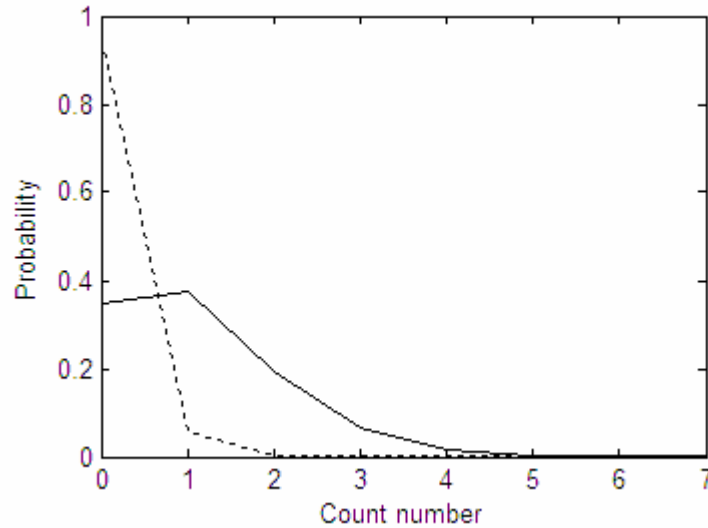


Figure 3.12, Simulation of signal and background distribution at image number $N=30$, $f=0.1$, $p_d = 34.57\%$, $p_f = 0.2\%$, the total expectation photon number is approximate 1. The solid line represents signal with background, and the dotted line represents background.

At count number=1 the background probability is 0.057, while the signal probability is 0.37. The background probability is very small and negligible when count number is greater than 2, thus it can be considered to be 'good performance' under this condition.

Chapter 4 Photon counting with fluorophore in TIRF

Although the performance of the camera is not ideal, attempt is still made to perform photon counting with fluorescent beads in TIRF.

4.1 Instrument configuration

The instrument system is TIRF and TIRM combined [16], but only TIRF is used in this experiment. The TIR system employs prismless configuration. A Meiji (Axbridge, Somerset, UK) TC5400 inverted biological microscope with a high-NA objective lens (Zeiss Plan-Fluar 100×1.45 NA) (Carl Zeiss Ltd., Welwyn Garden City, Hertfordshire, UK) formed the central component of the system, while a 488nm solid state laser (20mW, Protera 488-15, Novalux, Sunnyvale, CA) or a 532nm solid state laser (50mW, BWN 532-50, B&W TEK, Newark, DE) is used for TIRF light source.

Figure 4.1 shows the set-up of the system, L1-L2 and L3-L4 are used to expand the laser beam so a field of approximately $200\mu\text{m}^2$ can be illuminated on the object plane. L1 equals L3 and L2 equals L4, the focal length of L1 and L3 is 12mm and focal length of L2 and L4 is 250mm, thus the magnification is approximately 21X.

For the dual-colour TIRF illumination, 488nm and 532nm laser beam are combined at a dichroic beamsplitter DBS. The mirror and focusing lens L5 can be translated by the stage, so the position of the focal point in the back focal plane (BFP) of the microscope objective lens can be moved, therefore the incident illumination angle can be changed. Fluorescent emission and reflected LED illumination pass through the multi-band dichroic beamsplitter MDBS, and tube lens L10 forms an image on the EMCCD.

For 532nm excitation wavelength, the emission fluorescent wavelength is around 560nm, which is near the peak QE wavelength of the EMCCD, thus 532nm laser is used in the experiment. The sample is fluorescent beads of 170nm in size (540/560nm, Catalog Number: P7220, Molecular Probes, Inc.) The camera is connected to microscope via a 2.5X adapter (Meiji Techno UK Ltd.) and the magnification on the camera is approximate 250X. According to equation 1.2, with NA 1.45 and wavelength 560nm, the width of PSF is about 470nm, however since the size of beads (170nm) is not much smaller than width of PSF (470nm), the actual image size of the beads is the convolution of bead with PSF, and the image will be a little wider than 470nm. With magnification of 250X, length of 470nm on objective plane will be 117.5 μ m on CCD and occupy about 15 pixels (pixel size: 8 μ m).

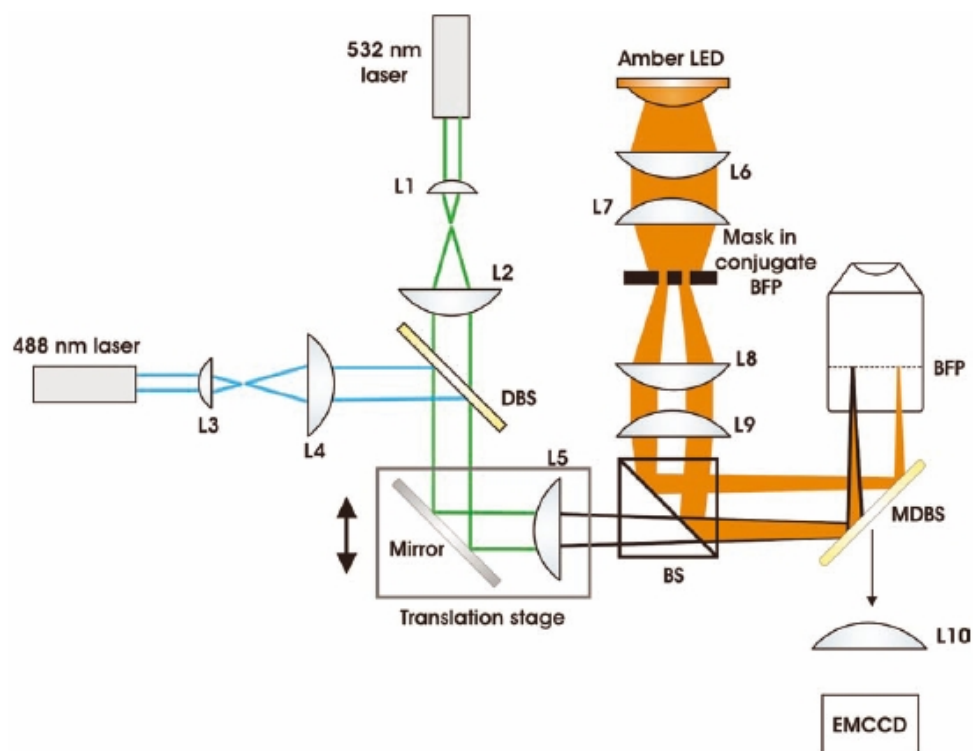


Figure 4.1 Schematic diagram of TIRF & TIRM combined system.

4.2 Method

The solution of fluorescent beads is diluted 1000 times before use. A droplet of solution is placed on a glass cover slip, then wait until the solution dry so the fluorescent beads are immobilized on the coverslip. A 50% ND filter is placed in front of laser so the emission light of fluorescent beads is strong enough for eyepiece observation and camera imaging without EM gain. Figure 4.2 shows an image of a fluorescent bead in this condition, the shape of point spread function is clear and some diffraction fringes are also visible. The positions of pixels with peak intensity of fluorescent bead image are recorded, and these pixels will be used for signal statistic in photon counting later on.

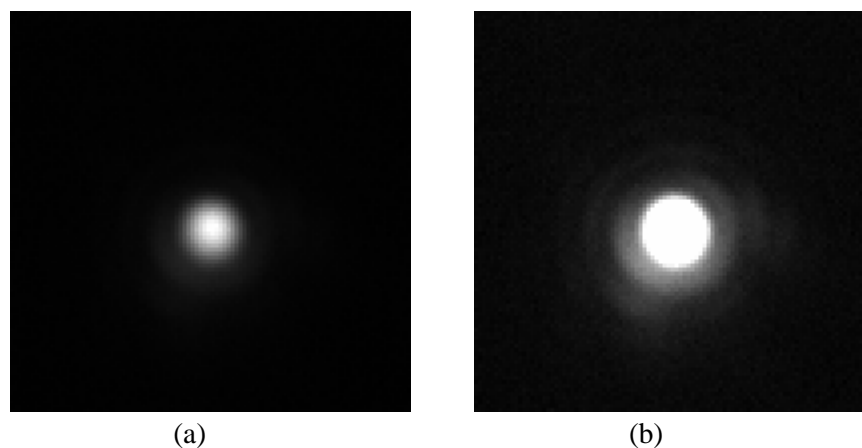


Figure 4.2 Image of a fluorescent bead under high intensity excitation beam. EM gain of camera is turned off. (b) is (a) with increased brightness to show sidelobe of the image.

After locating and focusing, another ND filter with attenuation factor of approximate 2000 is inserted and the EM gain of camera is turned on to perform photon counting.

The image acquisition of photon counting is almost the same as described previously, a small region (ROI, region of interest) containing one bead is selected, the camera is set to repeat exposure many times automatically (up to 10,000 times), and stacks of images are acquired. However since the emission intensity of beads is unknown, several exposure time are used so the mean intensity can be estimated. For each exposure time, two stacks of images are acquired, one for signal and one for background.

Baseline stability

In previous experiment with laser beam illuminating CCD, the option baseline clamp will result in signal shift (figure 2.5), thus the option was

turned off in that experiment. However the baseline stability is important for threshold processing and the drift of baseline will cause error. To determine whether the option baseline clamp is suitable for TIRF, an experiment is made to compare the result of imaging fluorescent bead with baseline clamp on and off.

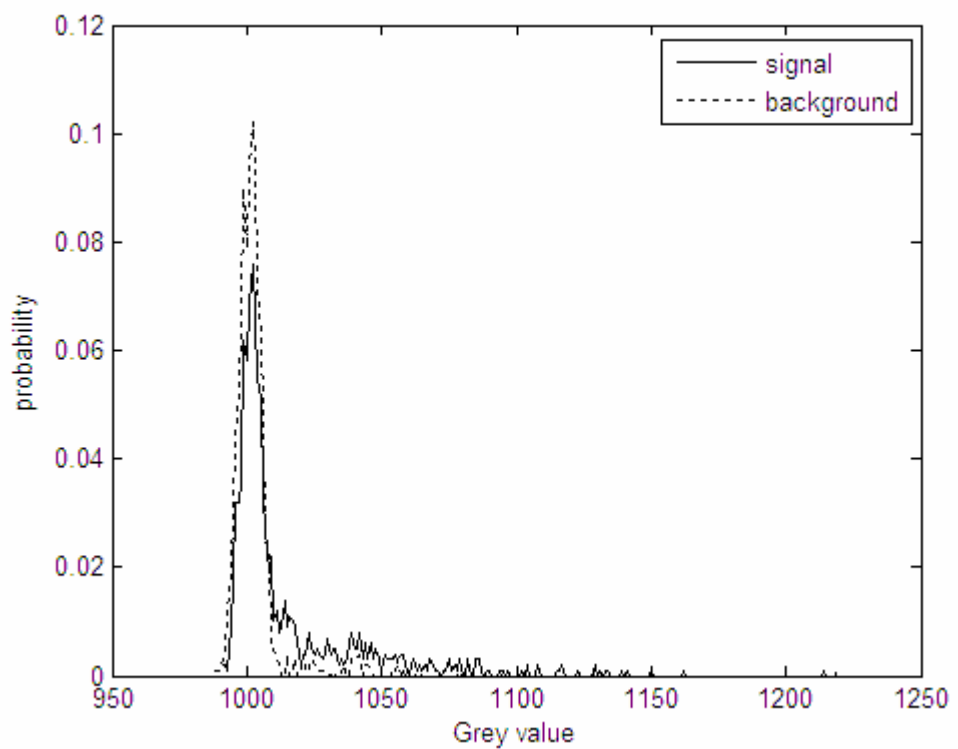


Figure 4.3 (a)

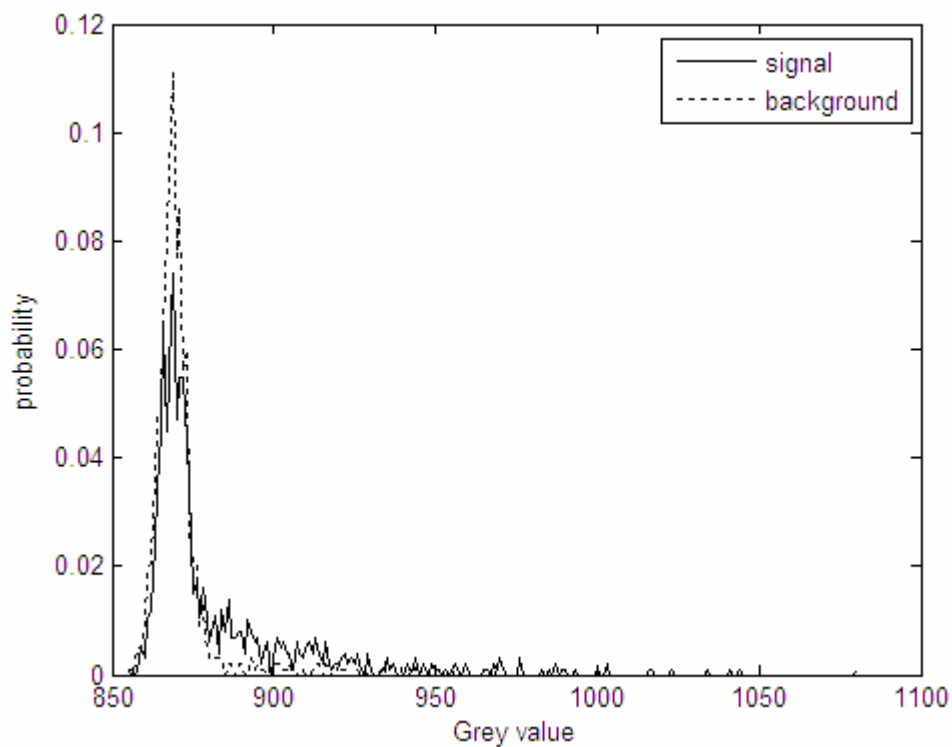


Figure 4.3 (b)

Figure 4.3 Statistical distribution of signal of one pixel with peak intensity of fluorescent bead, signal is extracted from a serial of 1000 images. Exposure time 100 ms. (a) Baseline clamp ON. (b) Baseline clamp OFF.

Figure 4.3 shows the signal distribution with option baseline clamp on and off, unlike figure 2.5, there is no difference between the two results. The signal distribution shift in figure 2.5 is probably because that all area of image is illuminated in previous experiment, while there is only a small area is illuminated in the fluorescent bead image, and perhaps the function baseline clamp needs a reference background to work properly. Since the option baseline clamp will not cause signal shift in TIRF, it is turned on in this experiment.

4.3 Analysis of results

After the images are acquired, the signals of peak intensity pixels are extracted from image stack. Table 4.1 shows the statistical data of a pixel signal.

Exposure time (ms)	10	50	100
Signal mean	1005.97	1008.98	1017.81
Background mean	1004.58	1003.59	1004.73
Signal std. deviation	14.36	20.04	29.37
Background std. deviation	10.96	12.21	13.54

Table 4.1 Mean and standard deviation of signal and background of one pixel at different exposure time.

According to table 4.1, the difference between signal mean and background mean at 100 ms exposure time is very close to that of light intensity 1 photon/pixel/exposure (Table 3.2), thus it is estimated that the light intensity on the pixel is approximate 1 photon/pixel/exposure at 100 ms exposure time, and 0.1 photon/pixel/exposure at 10 ms exposure time.

Light intensity of 0.1 photon/pixel/exposure is low enough for photon counting, so cumulative distribution function (CDF) of the pixel signal at 10ms exposure time is plotted for threshold value determination. Figure 4.4 shows the CDF, the probabilities of signal and background at various threshold values can be obtained from this CDF, and some probabilities are given in table 4.2.

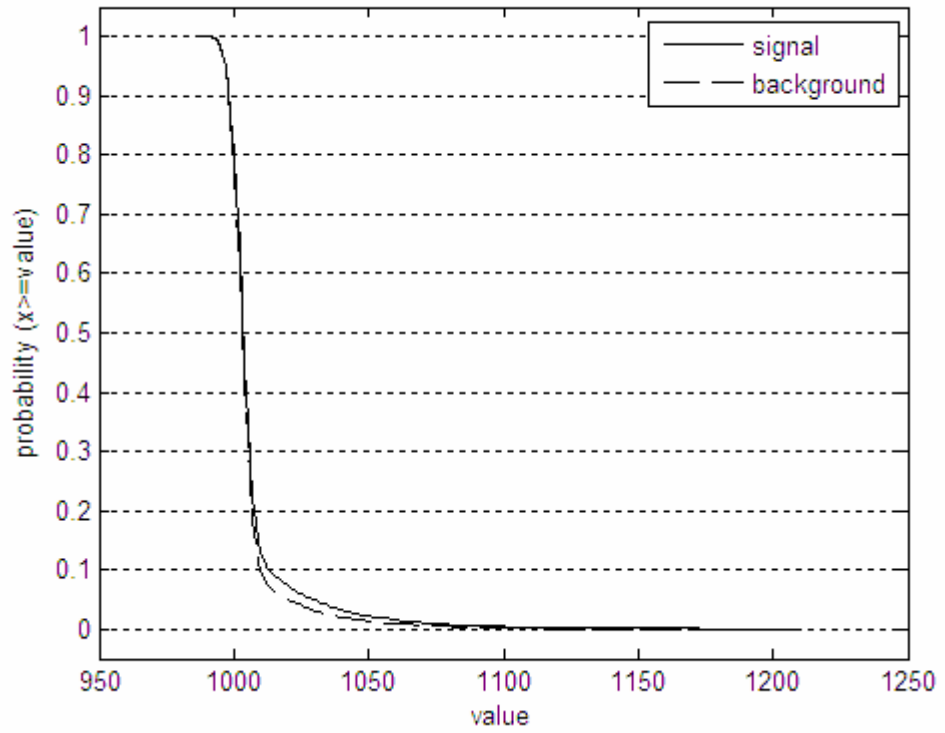


Figure 4.4 Cumulative distribution function of signal of a pixel with fluorescent bead peak intensity. Signal is extracted from a serial of 10,000 images, exposure time 10 ms.

Background probability	Threshold value	Signal probability
10%	1010	13.06%
5%	1020	7.38%
1%	1059	1.6%
0.5%	1078	0.81%

Table 4.2 Probability of background and signal at different threshold value.

To compare the results of different threshold value, three threshold values 1010, 1020 and 1059 are chosen for threshold processing. The threshold processing is simple, the image is analysed and all pixels with grey value higher than the threshold value are set to '1' and the other pixels are set to '0', thus the image is converted to a binary image. This step is applied to all images in the stack, so all 10,000 images are converted to binary image, then all these 10,000 images are summed up to form a final image.

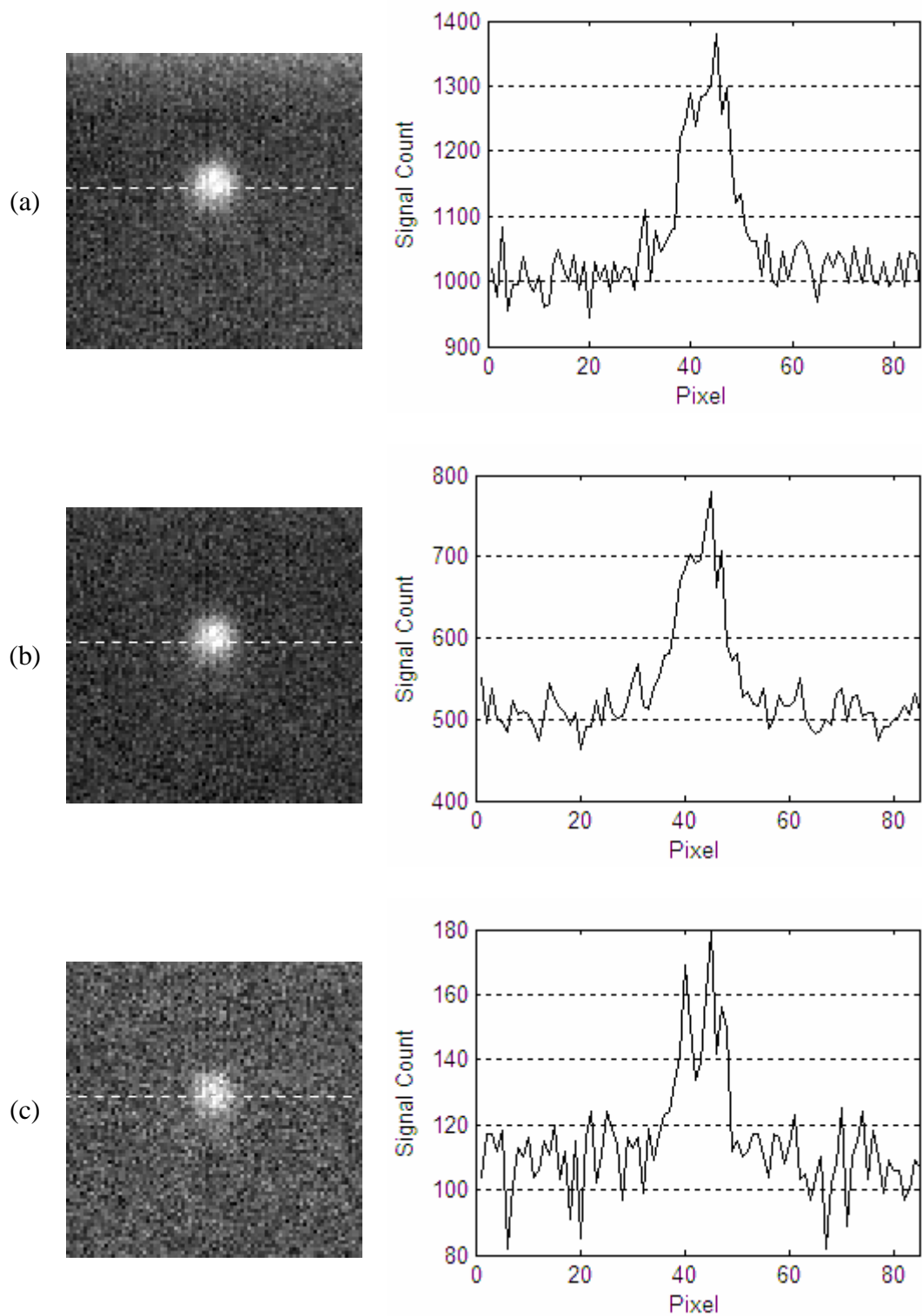


Figure 4.5 Resultant image of threshold processing at different threshold value.

Threshold value: (a) 1010; (b) 1020; (c) 1059.

Plot on the right is line profile of the dotted line on the corresponding left image.

The resultant images of threshold processing at various threshold values are shown in figure 4.5, the shape of fluorescent bead can be observed in the images, but the background is noisy, and the sidelobe cannot be detected, as predicted in previous simulation. The background in the images is due to the noise in EMCCD, the noise results in ‘false positive’ or ‘false count’ where there is no photon incident. The actual photon signal cannot be obtained by simply subtracting the background, because the background is not uniform and varies from pixel to pixel.

Although the background in the images is not uniform, it can be observed from the line profile of figure 4.5 that the background level fluctuates around a certain value which equals the product of background probability at corresponding threshold value (table 4.2) and total image number in the stack.

To study the variance of background in resultant image, the stack of 10,000 images for background (acquired in totally dark) is threshold processed, then the mean and standard deviation of the resultant image are calculated, as shown in table 4.3. According to the data in table 4.3, the mean and variance of resultant background image is very close, thus it can be assumed that the background noise obeys Poisson distribution.

Threshold value	Mean	Standard deviation (σ)	Variance (σ^2)
1010	991.23	32.44	1052.35
1020	511.44	22.51	506.70
1059	110.50	10.42	108.58

Table 4.3 Statistical data of background image after threshold processing at variant threshold value.

At a certain threshold value, let the probability of signal on a pixel be p , the probability of background on the same pixel be q , and the total image number in the stack is N . The mean value of signal count will be $p*N$, and the mean value of background count will be $q*N$. According to the assumption above, the background obeys Poisson distribution, and the standard deviation of background is $\sqrt{q*N}$. The actual photon signal is unknown, but it can be approximated by $(p-q)*N$, the difference between mean of signal and background. Thus the signal to noise ratio on resultant image of threshold processing can be express as:

$$SNR = \frac{(p-q)N}{\sqrt{qN}} = \frac{p-q}{\sqrt{q}} \sqrt{N} \quad (4.1)$$

It is obvious that the larger N , the higher SNR, and the coefficient $\frac{p-q}{\sqrt{q}}$ of the pixel on figure 4.4 can be calculated and plotted on figure 4.6. In figure 4.6, the coefficient is maximum (approximate 0.1) when threshold value is between 1010 and 1030, and the coefficient decreases as the threshold

value increases. The coefficient is meaningless as threshold value is above 1100, because the probability of signal and background are almost zero.

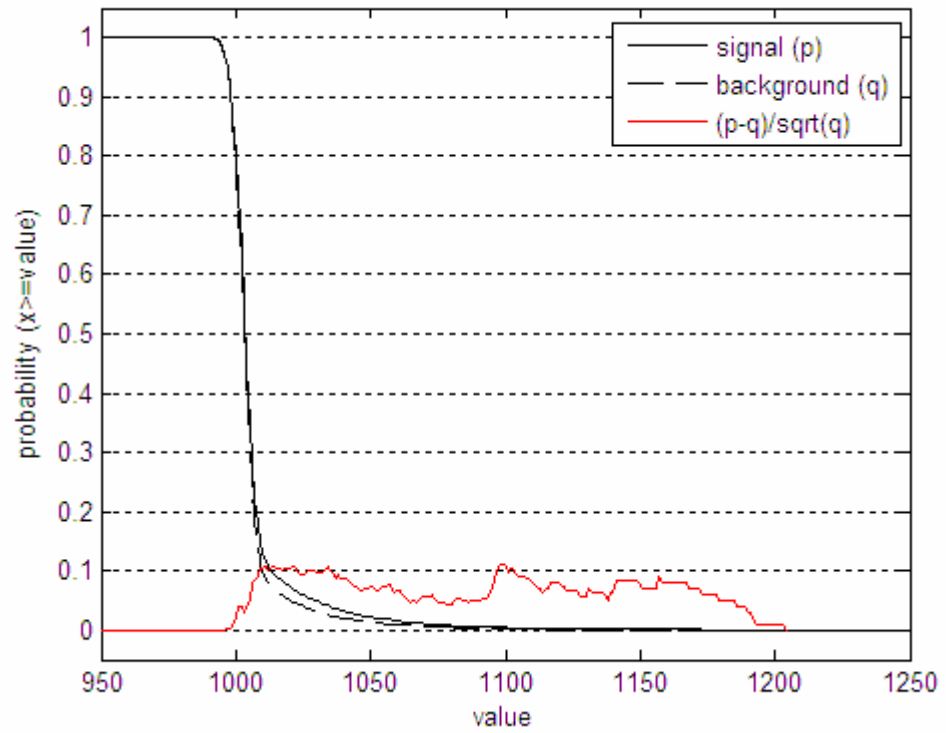


Figure 4.6 (a)

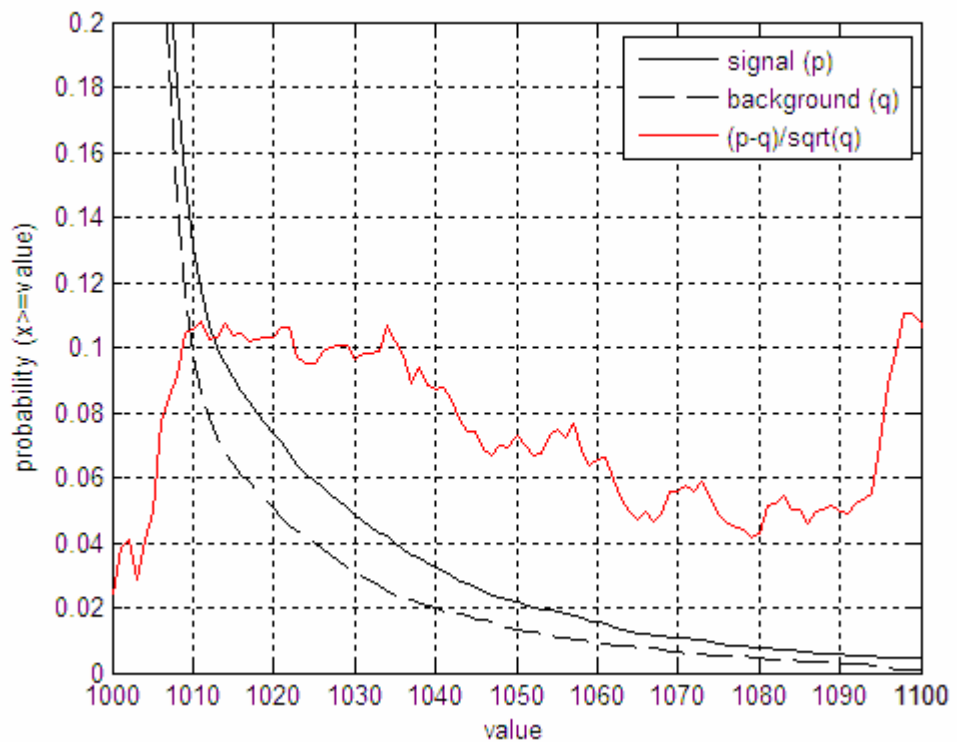


Figure 4.6 (b)

Figure 4.6 Curve of coefficient $\frac{p-q}{\sqrt{q}}$ of the pixel on figure 4.4. The

CDF of signal and background (blue and red line) are same as that in figure 4.4. (b) is an enlarged area in (a) to show detail of curve.

According to figure 4.6, the maximum coefficient value is approximate 0.1, for a stack of 10,000 images, the SNR is approximate 10, which is not a very low value. The greater the number of images, the more total photon signal count in resultant image, although the actual total photon signal count is unknown, it can be estimated by subtracting background mean value from signal. It is estimated that the total photon signal count in resultant image is approximate 25,000 at threshold value 1020 and approximate 50,000 at threshold value 1010.

However, if a smaller number of photons, for example several hundred to one thousand photons in each image, is required in Monte Carlo method, this requires much smaller number of image, and results in lower SNR. For example, at threshold value 1020, the number of image will be 400 if a resultant image with only 1,000 photon counts is needed, and the SNR of peak intensity in the image will be $0.1 * \sqrt{400} = 2$, this SNR is too low and can result in significant error. At this point of view, the noise in the camera is main problem in photon counting, so my conclusion is that the camera is not ideal for photon counting and STF measurement cannot be performed with this camera.

Moreover, the total time of image acquisition will be long under this condition. Leaving alone the SNR problem, a resultant image with 1,000 photon counts requires 400 exposures as described above, and tens of thousands of such resultant images are needed in Monte Carlo method. For example, to obtain 5,000 resultant images, 2,000,000 exposures are required. The camera needs approximate 4 minutes to complete 10,000 exposures, thus the total time for 2,000,000 exposures will be 800 minutes, or 13.3 hours. During such a long time, the fluorescent beads might suffer photobleaching, although the fluorescent beads are excited at very low intensity.

Chapter 5 Conclusion

5.1 Summary and conclusion

In this project, attempt is made to perform photon counting which can be used to measure stochastic transfer function (STF) by Monte Carlo method. In the Monte Carlo method, images of a point source containing only several hundred or thousands photons are required, a large number of such images are collected and Fourier transformed, and the mean and variance of distribution at each spatial frequency of the imaging system can be recovered, thus the STF can be obtained.

An EMCCD camera, which is supposed to have photon counting sensitivity, is used as photon counting device in the experiment. However, although it has been optimized, the EMCCD camera is found to be not as sensitive as the manufacturer claimed during the experiment, and an experiment is carried out to evaluate the performance of the EMCCD camera. In the evaluation experiment, the camera is illuminated by a beam of laser with known intensity (very weak intensity, 0.1 photon/exposure/pixel for example) and the output signal and background noise of the camera is recorded and statistical data is obtained. Moreover, a simulation based on the experiment data gives the EMCCD output signal distribution under different conditions.

According to the experimental data and simulation results, the EMCCD camera cannot separate signal from background at low light intensity because of its background noise, thus it is turned out to be not suitable for photon counting.

Moreover, an experiment of photon counting in TIRF with fluorescent beads in which condition the practical STF measurement will be performed is also carried out. According to the experiment result, the EMCCD is able to separate signal from background at high light intensity, but unable to separate at low intensity, which match the prediction of the simulation.

Therefore the conclusion about the EMCCD camera used in this project is that it is not capable of performing photon counting for the Monte Carlo method due to the noise of the EMCCD.

Although the attempt for photon counting was not successful, the performance of this EMCCD camera is studied, the evaluation method and data can be used as reference for evaluating other EMCCD or photon counting devices.

5.2 Other devices which might have better performance

Although the EMCCD used in this project is not suitable for photon counting, there are other types of devices which might provide better performance for photon counting, and might improve the measurement.

5.2.1 Back-illuminated EMCCD

The back-illuminated CCD is a CCD that has been reduced in thickness by etching and light falls onto the back of the CCD. Since the photon losses due to gate channel structures are completely eliminated, the back-illuminated CCD has higher quantum efficiency (QE) than normal CCD.

What is more important, some models of top performance back-illuminated EMCCD have very low Clock Induced Charge (CIC), which is important for photon counting. As described previously, CIC is a noise source in EMCCD and can be amplified by EMCCD gain register, thus it is important for EMCCD to keep CIC low.

According to Andor's document [17], their back-illuminated EMCCD have lower CIC than normal EMCCD. Figure 5.1 shows a line profile of image taken in totally dark by Andor's back-illuminated EMCCD and the EMCCD used in this experiment at high EM gain. The peaks in line profile represent CIC, thus it is clear that back-illuminated EMCCD has a lower

CIC level. A lower CIC level means lower noise and less ‘false count’ in threshold processing, which is very useful for photon counting.

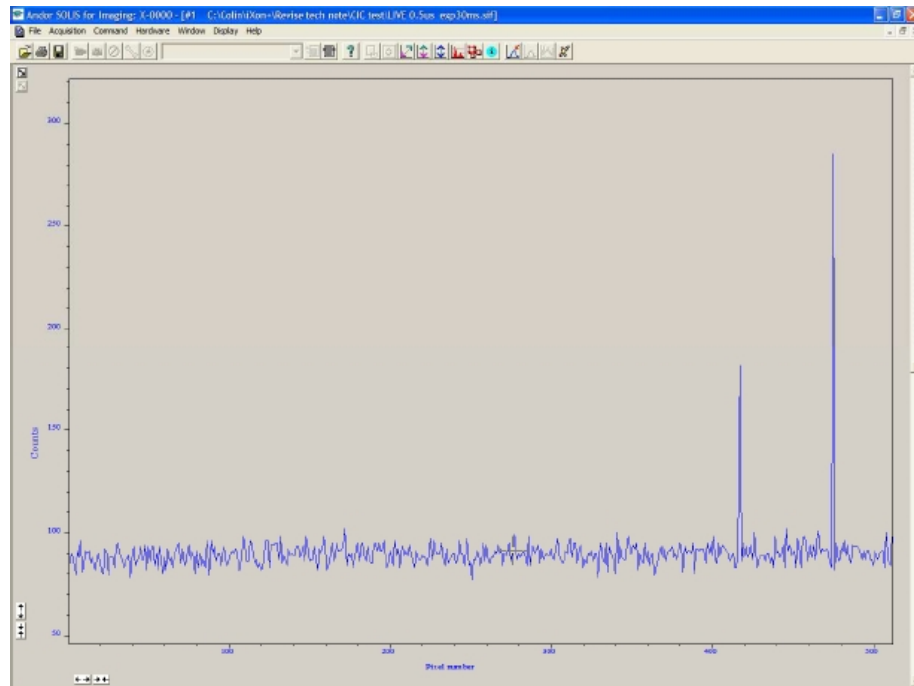


Figure 5.1 (a)

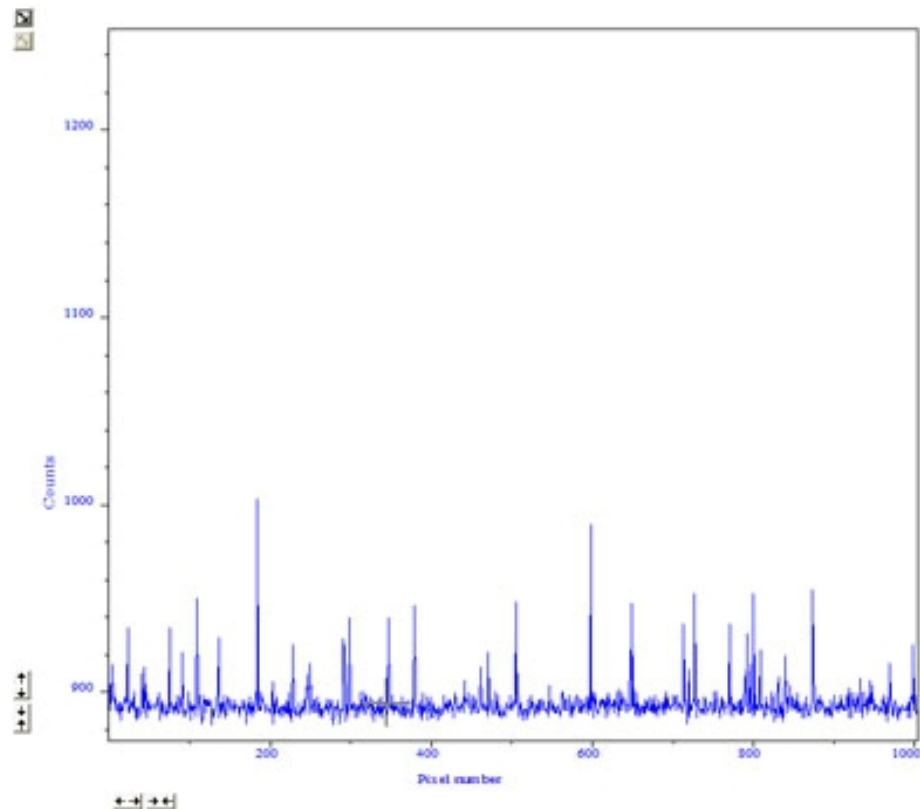


Figure 5.1 (b)

Figure 5.1 A line profile of dark image of different EMCCD at high EM gain. (a) Andor's back-illuminated EMCCD, copied from Andor's document. (b) EMCCD used in this experiment.

5.2.2 PMT

Photomultiplier tube (PMT) is very sensitive detector of light, and it has the capability of photo detection. However, PMT is usually used as point detector, and a scanning mechanism is need for 2D imaging. Because of the scanning mechanism, the image acquisition speed of PMT is usually slower than CCD. Moreover, PMT is usually bulky so huge magnification is needed to magnify the image of PSF for detection. Thus PMT is not very suitable for the application of STF measurement.

5.2.3 ICCD

An intensified charge-coupled device (ICCD) is a CCD that is optically connected to an image intensifier. The micro-channel plate (MCP), which is the core component of the image intensifier, can multiply electrons generated by a photocathode when photon incident. ICCD is also a very high sensitive detector of light and capable of photo detection, thus it has the potential of photon counting for STF measurement. However, actual performance evaluation is needed to confirm whether ICCD is really suitable for STF measurement.

References

1. Heintzmann, R. and G. Ficz, Breaking the resolution limit in light microscopy. *Brief Funct Genomic Proteomic*, 2006. 5(4): p.289-301.
2. Somekh MG, Hsu K, Pitter MC. (2008) Resolution in structured illumination microscopy: a probabilistic approach. *Journal of the Optical Society of America A: Optics, Image Science, and Vision*. Volume: 25 Issue: 6 Pages: 1319-1329.
3. <http://www.microscopyu.com/articles/digitalimaging/ccdintro.html>
4. <http://membres.lycos.fr/srondeau/ccd.htm>
5. http://www.andor.com/learning/digital_cameras/?docid=325
6. Axelrod, D. (1981) Cell–substrate contacts illuminated by total internal reflection fluorescence. *J. Cell Biol.* 89, 141–145.
7. Truskey, G.A., Burmeister, J.S., Grapa, E. & Reichert, W.M. (1992) Total internal reflection fluorescence microscopy (TIRFM) (II). Topographical mapping of relative cell/substratum separation distances. *J. Cell Sci.* 103, 491–499.
8. Hornung, J., Müller, T. & Fuhr, G. (1996) Cryopreservation of anchorage dependent mammalian cells fixed to structured glass and silicon substrates. *Cryobiology*, 33, 260–270.
9. Sund, S.E. & Axelrod, D. (2000) Actin dynamics at the living cell submembrane imaged by total internal reflection fluorescence photobleaching. *Biophys. J.* 79, 1655–1669.
10. Thompson, N.L., Drake, A.W., Chen, L. & Broek, W.V. (1997) Equilibrium, kinetics, diffusion and self association of proteins at membrane surfaces: measurement by total internal reflection fluorescence microscopy. *Photochem. Photobiol.* 65, 39–46.
11. Betz, W.J., Mao, F. & Smith, C.B. (1996) Imaging exocytosis and endocytosis. *Curr. Opin. Neurobiol.* 6, 365–371.

-
12. Oheim, M., Loerke, D., Stühmer, W. & Chow, R.H. (1998) The last few milliseconds in the life of a secretory granule. *Eur. J. Biophys.* 27, 83–98.
 13. Axelrod, D. (2003) Total internal reflection fluorescence microscopy in cell biology. *Biophoton. Pt B Methods Enzymol.* 361, 1–33.
 14. <http://www.microscopyu.com/articles/fluorescence/tirf/tirfintro.html>
 15. <http://www.andor.com/pdfs/specs/L885SS.pdf>
 16. G. D. Byrne, M. C. Pitter, J. Zhang, F. H. Flacone, S. Stolnik & M. G. Somekh. (2008) Total internal reflection microscopy for live imaging of cellular uptake of sub-micron non-fluorescent particles. *Journal of Microscopy*, Vol. 231, Pt 1 2008, pp. 168 – 179.
 17. <http://www.andor.com/pdfs/iXon> BI Tech Note 6pg 14Feb1r.pdf